MS version: 07-02-2023

Structural stability of the oyster gut microbiome contributes to the host's physiological tolerance to temperature fluctuations on tropical rocky shores

Bovern Suchart Arromrak[1]; Adrian Tsz Chun Wong[1]; Tin Yan Hui[1]; Kin Sum Leung[1]; Gray A. Williams[1]; Monthon Ganmanee[2]; Thierry Durand[3], Jetty Chung Yung Lee[4]; & Juan D. Gaitan-Espitia[1*]

[1] The Swire Institute of Marine Science and School of Biological Sciences, The University of Hong Kong, Hong Kong, SAR, China.

[2] Department of Animal Production Technology and Fisheries, Faculty of Agricultural Technology, King Mongkut's Institute of Technology Ladkrabang, Bangkok 10520, Thailand

[3] Institut des Biomolécules Max Mousseron (IBMM), Pôle Chimie Balard Recherche, UMR 5247, Université de Montpellier, CNRS, ENSCM, F-34293 Montpellier Cedex 05, France

[4] School of Biological Sciences, The University of Hong Kong, Hong Kong, SAR, China

*** Correspondence**: juadiegaitan@gmail.com

Abstract

Extreme thermal conditions on rocky shores are challenging to the survival of intertidal ectotherms, especially during emersion periods. Yet, many species are highly successful in these environments in part due to their ability to regulate intrinsic mechanisms associated with physiological stress and their metabolic demands. More recently, there has been a growing awareness that other extrinsic mechanisms, such as animal-associated microbial communities, can also influence the tolerance and survival of ectotherms under stressful conditions. The extent to which intrinsic and extrinsic mechanisms are functionally linked as part of the overall adaptive response of intertidal animals to temperature change and stress is, however, poorly understood. Here, we examined the dynamics and potential interactions of intrinsic and extrinsic mechanisms in the ecology of the tropical high shore rock oyster, *Isognomon nucleus*. We found that oysters modulate their internal biochemistry (PUFA-oxidised metabolites including 5-F_{2t}-IsoP, 10-F_{4t}-NeuroP, 13-F_{4t}-NeuroP, and 16-F_{1t}-PhytoP) as part of their adaptive regulation to cope with physiological stress during periods of extreme temperatures when emersed. While we detected extrinsic microbiome changes in alpha diversity, the overall taxonomic and functional structure of the microbiome showed temporal stability with no association with the host biochemical profiles. Our finding here suggests that the microbiome taxonomic and functional structure is maintained by a stable host control (not associated to the host biochemistry) and/or that the microbiome (independent of the host) is resilient to the temperature fluctuations and extremes. This microbiome stability is likely to contribute to the oyster, *I. nucleus* thermal tolerance, in addition to the intrinsic biochemical adjustment, to survive in the thermally challenging intertidal environment.

Introduction

The tropical rocky shore is one of the most extreme environments on Earth. This system is characterised by a marked heterogeneous thermal landscape influenced by tidal dynamics (Helmuth and Hofmann, 2001; Raffaelli and Hawkins, 1999). Across this vertical gradient defined by the tides, environmental temperatures shape the physiology, behaviour, and spatial distribution of tropical intertidal ectotherms (Chow, 2004; Garrity, 1984; Giomi et al., 2016; Ng et al., 2017; Samakraman et al., 2010; Williams and Morritt, 1995). For ectotherms occupying the high shore habitat, thermal and oxidative stress (i.e., excessive production of reactive oxygen species - ROS) during desiccation periods of extended emersion, are the two major physiological challenges faced (Birben et al., 2012; Freire et al., 2011; Sokolova and

65 Pörtner, 2001). To survive under these challenging conditions, high shore intertidal ectotherms
66 modulate intrinsic mechanisms associated with their internal physiology (e.g., metabolic rate)
67 and biochemical activities. This modulation can be observed through, for instance, the
68 regulation of ROS level via polyunsaturated fatty acids (PUFA; Letendre et al., 2009; Sokolova
69 and Pörtner, 2001; Wang et al., 2018; Yin et al., 2017), and/or the control of the gene expression
70 associated with heat shock response (HSR) and oxidative stress response (OSR; Wang et al.,
71 2022). In addition to that, some of these organisms are able to enter into a hypometabolic state
72 (i.e., metabolic depression; Hui et al., 2020; Marshall and McQuaid, 2011) to avoid excessive
73 energy consumption when exposed to high temperatures during low tides. Together, these
74 functional characteristics are regarded as important, adaptive traits for intertidal ectotherms to
75 cope and ameliorate the extreme stress experienced on tropical rocky shores.
76 Survival under stressful environmental conditions is also hypothesized to be influenced
77 by extrinsic mechanisms such as host-associated microbial communities (i.e., microbiome;
78 Ahmed et al., 2019; Bang et al., 2018; Fan et al., 2013). The structure and functions of these
79 microbiomes have been suggested to play important roles in shaping tolerances and
80 biochemical regulation of animals to elevated temperatures (Herrera et al., 2020; Moghadam et
81 al., 2018; Tignat-Perrier et al., 2022). Under such conditions, functional microbiomes that are
82 resilient/responsive to environmental changes are fundamental to the host's health and survival
83 (Klepac et al., 2015; Kremer et al., 2018; Muñoz et al., 2019; Soen, 2014). For instance, Epstein
84 et al. (2019) demonstrated that the resilience of the coral, *Pocillopora acuta,* to a stressful
85 thermal event may be attributed to the stability of the microbiome composition and structure.
86 In contrast, a dysbiotic host state is commonly associated with a breakdown in microbiome
87 stability (Fan et al., 2013; McDevitt-Irwin et al., 2019). This is typically reflected by a marked
88 variation among host-associated microbiomes, a signal indicating the host losing control of the
89 microbial community and/or differential sensitivities of microbiomes to extreme disturbances
90 (Carey and Duddleston, 2014; Lokmer and Mathias Wegner, 2015; Zhou et al., 2014). This
91 pattern is in-line with the "Anna Karenina Principle", which states, "all happy families are all
92 alike; each unhappy family is unhappy in its own way" (Díaz-almeyda et al., 2022; Pita et al.,
93 2018; Zaneveld et al., 2017). In other words, stressed organisms may host more stochastic
94 microbiomes than healthy organisms. Although microbiome stability seems important for the
95 correct functioning of the host, some studies have suggested that flexibility in the microbiome
96 can also provide adaptive capacities to the host, allowing it to cope with rapidly changing
97 environments (Maher et al., 2020; Voolstra and Ziegler, 2020). Ziegler et al. (2017), for
98 example, showed that the coral *Acropora hyacinthus* exhibits changes in its microbiome

composition and structure that are aligned with the local thermal environmental conditions. Similarly, several studies have also shown seasonal variation in the host-associated microbiome of many marine organisms such as bivalves and echinoderms, as a potential plastic/flexible response to environmental change (Bäckhed et al., 2015; Feng et al., 2021; Pierce and Evan, 2019). Microbiome stability or flexibility may, therefore, be a sign of host adaptive responses to environmental changes. However, the influence of these contrasting patterns is context-dependent and thus, their contribution to the tolerances and survival of animal hosts may differ in extreme environments such as tropical rocky shores.

Previous studies have shown that the capacity for plastic adaptive responses of animal hosts to environmental stress may be modulated by the interactions between intrinsic (physiology and biochemical changes of the host) and extrinsic (host's microbiome structure and function) mechanisms (Fontaine and Kohl, 2022; Marangon et al., 2021; Muñoz et al., 2019; Walke et al., 2021). It is unclear, however, to what extent these mechanisms are functionally linked as part of the whole organism's adaptive response to survive in an extreme environment such as the tropical intertidal rocky shore. In this study, we investigated the intrinsic and extrinsic mechanisms underpinning tolerances and survival of a tropical intertidal ectotherm (oyster *Isognomon nucleus*) by assessing the influence of natural variation in environmental temperature on i) host physiology (i.e., biochemical dynamics) ii) the diversity, structure, and function of the host-associated microbiome and iii) the interplay between these mechanisms. The integration of intrinsic and extrinsic mechanisms offers a holobiont perspective for understanding the stress tolerance regulation of ectotherms in extreme and fluctuating environments (Alberdi et al., 2016; Apprill, 2017; Bang et al., 2018).

Material and Methods

Site and species descriptions

Host-microbiome interactions were investigated in the high shore intertidal oyster, *Isognomon nucleus* (Bivalvia: Isognomonidae). Animals were collected from Ko Sichang, Thailand (latitude: 13°08'52''N; longitude: 100°48'11''E, (Samakraman et al., 2010). In this area, *I. nucleus* is abundant and forms a distinctive band at the supra-littoral region (~2.5 - 3 m above the mean sea level; Samakraman et al., 2010), where rock temperatures vary daily (emersion period) from ~30°C at dawn to ~50°C at noon (hot season: March to June; Hui et al., 2020). The oyster exhibits strong variations in physiological and metabolic adjustments with elevated body temperatures, providing an ideal system to investigate the functional role of the

132 microbiome to facilitate the host's survival in this thermally extreme and variable environment
133 (Giomi et al., 2016; Hui et al., 2020).
134

135 *Sample collection and processing*

136 A total of 80 individuals of *I. nucleus* were randomly selected at four different
137 timepoints within an emersion period (Fig. 1A; 20 animals at each time) with contrasting
138 thermal conditions (09:15 hr, 12:30 hr, 16:12 hr, and 17:40 hr; hereafter, morning, noon, early-
139 afternoon, and late-afternoon, respectively; Table S1). This cycle represents major changes in
140 the environmental temperature as a result of the tidal dynamics and air/sun exposure (Hui et al.,
141 2020). Body temperatures were measured from 10 randomly selected individuals at each
142 timepoint using a digital thermometer (± 0.1 ˚C, TM-947SD, Lutron, Taiwan) where a fine-
143 tipped type-K thermocouple was inserted into the bodies through the valve opening. At each
144 time point, the whole tissue of five collected oysters was quickly removed at the site with a
145 sterile dissecting kit and snap-frozen in liquid nitrogen on shore for oxidative stress
146 quantification (as a proxy for host physiological and biochemical dynamics). The guts of
147 another five individuals were also dissected at each timepoint on-site, snap frozen in liquid
148 nitrogen for gut microbiome assessment. All collected samples (20 for oxidative stress and 20
149 for microbiome analysis across four time points) were stored in a portable liquid nitrogen tank
150 and transported to The University of Hong Kong within three days, where they were held in a
151 -80°C freezer until processing and analyses.
152

153 *Rock surface temperature and tidal dynamics*

154 To quantify environmental conditions experienced by *Isognomon nucleus* throughout
155 the tidal cycle, rock surface temperatures and tidal levels were recorded. To measure and track
156 surface rock temperature, i-Button loggers (DS1922L, Maxim, US) were firstly embedded in
157 waterproofing resin (Scotchcast, 3M, US), placed in plastic Falcon tube caps and affixed, using
158 marine epoxy (A-788, Z-Spar, US; Ng et al., 2021), onto the shore at the height where *I. nucleus*
159 were collected. Rock surface temperatures were logged by these i-Buttons every 5 minutes at a
160 resolution of 0.5 °C (n = 5). Additionally, a time-lapse camera (TLC200Pro, Brinno, Taiwan)
161 was set adjacent to the study site to monitor the immersion state of the *I. nucleus* band during
162 the day (~ 05:00 hr to 18:00 hr) to assess the tidal states. Images were captured every 10 minutes
163 and the tidal level was scored according to whether the band was underwater (immersed),

164 exposed to air (emersed), or being splashed by waves during transitions from
165 immersion/emersion (awash).
166

167 *Determination of polyunsaturated fatty acids-oxidised metabolites*
168
169 The levels of oxidative stress (i.e., associated with ROS production) of the oysters were
170 determined based on the concentration of non-enzymatic polyunsaturated fatty acids (PUFA)-
171 oxidised metabolites (hereafter, PUFA-oxidised metabolites; Basu, 2010; Durand et al., 2009;
172 Leung et al., 2015). A modified Folch extraction method was used to extract the PUFA-oxidised
173 metabolites from the oysters sampled (n=5) at each timepoint (t=4) (Dupuy et al., 2016; Folch
174 et al., 1957). In brief, 0.05g of oyster flesh was suspended in a 5 ml ice-cold Folch solution
175 (chloroform: methanol, 2:1, v/v) with 0.01% BHT (w/v) and homogenized at 24,000 rpm in 20
176 secs bursts on ice using a polytron benchtop homogenizer (T25, Ultra-Turrax, IKA, Germany).
177 Homogenization was performed twice, and the two parts of the Folch solution extracts were
178 pooled. The pooled solutions were added with 2 ml of 0.9% NaCl to introduce phase separation.
179 The mixture was then shaken on ice for 30 min and centrifuged at 2000 × g for 10 min at room
180 temperature. The lower chloroform phase was transferred into a 30 ml glass vial. The extracted
181 samples were then added with potassium hydroxide (1M in methanol) and 1X PBS (pH7.4).
182 Samples were then shaken overnight in the dark at room temperature for alkaline hydrolysis.
183 The reaction was terminated by adding 1M of hydrochloric acid, methanol, 20 mM of formic
184 acid, and 40 mM of formic acid. Deuterated internal standards (5ng prepared in methanol) were
185 also added after the hydrolysis. Purification of the oxidised PUFA metabolites was performed
186 with the mixed anion solid phase extraction (MAX SPE, Waters, Milford, MA USA). Before
187 the start of the solid phase extraction, the SPE column was preconditioned with methanol and
188 20 mM formic acid. One sample was then loaded into a column and cleaned with 2%
189 ammonium hydroxide and 20 mM formic acid. The final eluent was collected with
190 hexane/ethanol/acetic acid (70/29.4/0.6, v/v/v). All the samples were then placed on a heating
191 block and heated at 37°C under a stream of nitrogen gas until they were completely dried. The
192 dried samples were then re-suspended in 100 µL methanol and cleaned through a 0.45 µm PTFE
193 filter to remove insoluble impurities, and then immediately analysed by liquid chromatography-
194 tandem mass spectrometry (LC-MS/MS).
195 In our study, we used the Sciex X500R QTOF LC-MS/MS system (Sciex Applied
196 Biosystems, MA, USA) which consisted of an Exion LC liquid chromatography with a C18
197 column (150×2.1 mm, 2.6 µm particle size, Phenomenex, Torrance, CA, USA) which was

198 maintained at 40°C for LC-MS/MS analysis. A mobile phase consisting of 0.1% aqueous acetic
199 acid (solvent A) and 0.1% acetic acid/methanol (solvent B) was used. The flow rate was set to
200 300 µl/min and the injection volume to 10 µl. For each sample analysis, the gradient condition
201 was maintained at 20% of solvent B for 2 min and between 20% and 98% for 8 min and then
202 held for 5 min. Then, the percentage of solvent B was reduced to 20% in 1 min and held for an
203 additional 5 min to equilibrate to the initial conditions. The X500R QTOF system was operated
204 in negative electrospray ionization (ESI) mode. The spray voltage was set to -4500V and
205 nitrogen was used as the curtain gas. The ionization chamber temperature was set at 350°C, and
206 the pressure of the ion source gases 1 and 2 were 35 and 45 psi, respectively. The declustering
207 potential (DP) was set to -80V and the collision energy (CE) was -10V for the QTOF MS. The
208 scan mode was set to multiple reaction monitoring (MRM). All data collected by the X500R
209 QTOF system was analyzed by the Sciex operating system (version 1.2.0.4122). The
210 quantification of each analyte was determined by correlating the peak area to its corresponding
211 deuterated internal standard peak. For analytes without corresponding deuterated internal
212 standards, the following deuterated internal standards, 5(*S*)-HETE-d_8, 15-F_{2t}-IsoP-d_4, and 4-F_{4t}-
213 NeuroP-d_4 were used for quantification. We identified fifteen PUFA-oxidised metabolites that
214 are known to be the products of non-enzymatic lipid peroxidation, based on previous work by
215 Dupuy et al.(2016), Galano et al.(2017) and Lee et al.(2018). These metabolites were derived
216 from the oxidation of the following PUFA: (1) Arachidonic acid (ARA) (2) Adrenic acid (AdA)
217 (3) Docosahexaenoic acid (DHA) (4) α-Linolenic acid (ALA) (5) Eicosapentaenoic acid (EPA).
218

219 *DNA extraction and 16S rRNA gene sequencing*

220 Total genomic DNA was extracted from the oysters' guts (~0.03g) using the commercial
221 DNA extraction kit, Dneasy Power Soil Kit (Qiagen GmbH, Hilden, Germany), following the
222 manufacturers protocol with some modifications (i.e., the solution mixture was incubated at 55°C
223 in a water bath for 30 minutes after the bead-beating step). The extracted DNA (100µl) was
224 then collected in a microcentrifuge tube and preserved in a -80°C freezer. All the DNA samples
225 were then sent to Ramaciotti Centre for Genomics at the University of New South Wales,
226 Sydney Australia for 16S rRNA amplicon paired-end sequencing (2X 300bp) on an Illumina
227 Miseq Platform. Before the amplicon sequencing, the V3-V4 variable region of the 16S rRNA
228 gene from each DNA sample was amplified using the following primers: (1) 341F (Forward
229 Primer);5'- CCTACGGGNGGCWGCAG-3' (2) 805R (Reverse Primer); 5'-
230 GACTACHVGGGTATCTAATCC-3'(Herlemann et al., 2011; Klindworth et al., 2013). Raw

231 reads received were the demultiplexed paired-end sequences in a FASTQ format and they were
232 deposited in NCBI Sequence Read Archive (SRA) under Bioproject number PRJNA931123.
233 The data will be made available once published.
234

235 *16S rRNA gene sequence processing*

236 Raw demultiplexed paired-end sequences were processed following the Quantitative
237 Insights into Microbial Ecology (QIIME2 ver. 2021.4) pipeline (Bolyen et al., 2019). Briefly,
238 the raw data was first visualized with the demux plug-in function for quality-checking and
239 identifying poor-quality base regions to filter. The sequences were then trimmed, filtered,
240 denoised, chimeras-removed, and merged using the DADA2 plug-in function in QIIME2
241 (Callahan et al., 2016). The sequences were identified at a single nucleotide threshold
242 (Amplicon Sequence Variants; ASV; Callahan et al., 2017). Additional steps of quality control
243 were performed to reduce non-target sequences by aligning (vsearch alignment method) the
244 ASV sequences to the 99% representative sequences from the greengenes database and only
245 ASV with a similarity threshold of 0.65% and coverage threshold of 0.5% were retained
246 following https://github.com/biocore/deblur/issues/139#issuecomment-282143373. Singletons
247 and sequences with less than 349bp were also removed with filter-features and filter-sets
248 function in QIIME2, respectively. The quality-filtered sequences were then taxonomically
249 assigned with a naïve-Bayes classifier trained on the V3-V4 region of the 16S gene in the Silva
250 v138 database (Quast et al., 2013), using the classify-sklearn function in the feature-classifier
251 plugin (Bolyen et al., 2019). The output from this generated a taxonomy table with taxonomic
252 naming for each ASV found within our samples. ASV sequences that were identified as
253 mitochondria, chloroplast, archaea, and eukaryotes were filtered out. The quality-filtered ASV
254 sequences were then ready to be used for downstream analysis.
255

256 *Profiling microbiome functions*

257 The functional microbiome was predicted using the software Phylogenetic Investigation
258 Communities by Reconstruction of Unobserved States version 2 (PICRUSt2; Douglas et al.,
259 2020). The predicted functions associated with the microbiome (using the quality-filtered
260 sequences) were inferred based on the MetaCyc pathway abundance, using the PICRUSt plug-
261 in within QIIME2.
262

263 *Data analysis*

264 Unless otherwise specified, the R statistical programming language (ver. 4.2.0, R Core
265 Team) and R Studio was used to generate graphics and statistical analyses. The oysters' body
266 temperature data violated the statistical assumption of homogeneity of variances (Levene's test,
267 p-value < 0.05). Hence, the statistical analysis for this trait across different timepoints was
268 assessed using a generalized linear model (GLM) with a gamma distribution. The likelihood-
269 ratio chi-square test was used to determine the statistical significance and is indicated if the p-
270 value was < 0.05 (R package "Car"; Fox and Weisberg, 2019). Post-hoc testing for pairwise
271 comparison was made using the estimated marginal means with Tukey's tests from the R
272 package emmeans (Lenth, 2023)

273 Individual PUFA-oxidised metabolites were first evaluated for normality (Shapiro-
274 Wilk's Test) and homogeneity of variance (Levene's test) assumptions. Metabolites that
275 fulfilled both assumptions were tested with one way Analysis of variance (ANOVA) to
276 investigate the variation in metabolites' concentrations across timepoints, followed by *post-hoc*
277 Tukey's Honest significant difference (Tukey's HSD). For metabolites that violated either one
278 of the assumptions, they were evaluated with GLM (gamma distribution) following a similar
279 procedure as with the body temperature datasets.

280 Assessment of PUFA-oxidised metabolites' beta diversity (with all the 15 metabolites
281 or only the 4 significant metabolites) was performed by first generating a Euclidean distance
282 matrix between samples. A principle Coordinate Analysis (PCoA) plot was then created to
283 visualize the PUFA-oxidised metabolites clustering across different timepoints, using the
284 ggplot2 R package (Wickham, 2008). Permutational multivariate analysis of variance
285 (PERMANOVA) was performed with 999 permutations to test for the differences in PUFA-
286 oxidised metabolites profile across timepoints (Oksanen et al., 2022). We also performed a
287 permutational multivariate dispersion test (PERMDISP) to assess differences in the dispersion
288 of metabolite profiles between timepoints with 999 permutations followed by pairwise
289 comparisons. All multivariate metabolites analyses were performed using the package vegan in
290 R (Oksanen et al., 2022).

291 Oysters' gut microbiome analysis was conducted by first combining the ASV count data,
292 taxonomy table, and metadata into a simplified data matrix for ease of downstream processing,
293 using the phyloseq() function from the phyloseq R package (McMurdie and Holmes, 2013).
294 Rarefaction curves (total ASVs captured against sampling depth) were generated for each
295 sample with the ggrare() function from the ranacapa R package (Kandlikar et al., 2018). All

296 samples approached the asymptote level, indicating that the total ASV richness for each sample
297 has been captured (Fig. S1). Each of the samples was then rarefied to a sampling depth of
298 21,282 reads (a cut-off that balances the maximum number of sequences retained per sample
299 and minimizing the number of samples removed) for downstream analysis (i.e., alpha and beta
300 diversity; McKnight et al., 2019; Weiss et al., 2017). Using the rarefied data, the microbiome
301 alpha diversity was determined based on two indices – ASV richness and Shannon-Wiener (H')
302 diversity. ASV richness was calculated with the Base-R function, while Shannon-Wiener (H')
303 diversity index was generated using the diversity() function from the Vegan package (Oksanen
304 et al., 2022). Differences in the microbiome alpha diversity across the timepoints were assessed
305 with ANOVA and followed by a *post-hoc* Tukey HSD test. The ANOVA statistical
306 assumptions of normality (Shapiro-Wilk test) and homogeneity of variance (Levene's test) for
307 all datasets were tested and fulfilled (p-value > 0.05). Linear regression analysis was also
308 conducted to determine the relationship between the oysters' microbiome alpha diversity (i.e.,
309 ASV richness and Shannon-Wiener (H') index) and body temperature (i.e., average of the 10
310 random independent body temperature replicates collected at each timepoint). The statistical
311 assumptions for the linear regression model were fulfilled based on the normality test (Shapiro-
312 Wilk test) and residuals plot (variance homogeneity).

313 Beta diversity of the oysters' gut microbiome taxonomic and functional profiles was
314 evaluated by generating the Bray-Curtis dissimilarity distance matrix between samples, and a
315 PCoA plot was then created to visualize microbiome taxonomic and functional clusters across
316 different timepoints, using the ggplot2 R package (Wickham, 2008). PERMANOVA was
317 performed with 999 permutations to test for the differences in the microbiome composition and
318 structure between timepoints (Oksanen et al., 2022). PERMDISP with 999 permutations was
319 performed to test for differences in the taxonomic and functional microbiome profile dispersion
320 followed by pairwise comparison. All multivariate analyses were conducted using the package
321 vegan in R.

322 For the microbial taxa profiling, the unrarefied quality-filtered ASV sequences were
323 binned to the family taxonomic level for each sample. Differential abundance analysis of
324 microbiome was performed with family taxonomic level data and analysed with Analysis of
325 Composition Microbiome with Bias Correction (ANCOM-BC) from the ANCOMBC R
326 package (Lin and Peddada, 2020; Nearing et al., 2022).

327 Mantel test (Spearman correlation method) was employed to determine the correlation
328 between the *I. nucleus* microbiome taxonomic structure and the PUFA-oxidised metabolites
329 using their dissimilarity matrices across timepoints using the mantel() function in vegan

330 package (Oksanen et al., 2022), which tested whether higher dissimilarity in microbiome was
331 associated with higher dissimilarity in metabolite profiles. Since the oysters' microbiome and
332 metabolites were sampled from independent individuals, we averaged each microbial taxon and
333 each metabolite concentration across replicates at each timepoints before generating a
334 dissimilarity distance matrix between samples – Bray-Curtis (microbiome) and Euclidean
335 (metabolites).
336 The GraphPad Prism software (San Diego, California, USA) was used to generate the
337 figure for oyster's body temperatures, individual PUFA-oxidised metabolites and the 10
338 dominant microbe's relative abundance across the timepoints.
339

340 # Results

341 *Tidal dynamics and temporal changes in environmental and body temperatures*

342 Oysters were regularly exposed to the air as a result of the tidal regime (Fig. 1A) and
343 this temporal change was aligned to changes in the rock surface temperature across the day,
344 with the highest temperature recorded at noon (45-50°C, Fig. 1A). The body temperature of the
345 oysters varied temporally (Fig. 1B; GLM $\mathcal{X}^2_{(3)} = 1073.9$, p-value < 0.05), increasing from 32.11
346 ± 0.12 °C (mean ± SD) in the morning to 39.99 ± 0.95 °C (mean ± SD) at noon, after which
347 body temperatures drop steadily to ~ 35 °C in the afternoon. Besides early-afternoon (35.4°C ±
348 0.46) and late-afternoon (35.18 °C ± 0.46), all pairwise comparisons showed significant
349 differences in body temperatures between timepoints. Such temporal variation in body
350 temperature encompasses the thermal window (noon's temperature) where oysters are expected
351 to enter a state of metabolic depression (body temperatures falling within the metabolic
352 depression range, i.e., cBP1 – cBP3; Fig. 1C), as well as windows where they remain active
353 (body temperatures before cBP1, Fig. 1C).
354

355 *Temporal assessment of PUFA-oxidised metabolites*

356 There was no significant difference in the metabolites profile (contributed by fifteen
357 metabolites) between timepoints (Table 2), but PERMDISP indicated a significant difference
358 in their dispersion (Table 3; Fig. 3A). Individual analyses revealed that only four PUFA-
359 oxidised metabolites (i.e., 5-F_{2t}-IsoP, 10-F_{4t}-NeuroP, 13-F_{4t}-NeuroP, and 16-F_{1t}-PhytoP)
360 significantly varied between timepoints (Table 1, Fig. 2). An additional PERMANOVA
361 analysis for these four metabolites showed a significant difference in the clusters between the
362 morning metabolites profile and all the other timepoints during the emersion period (Table 2;

363 Fig. 3B). Multivariate dispersion of the four PUFA-oxidised metabolites also differed between
364 timepoints (Table 3; Fig. 3B). With the exception of two pairwise comparisons (i.e., noon vs.
365 early-afternoon, and early-afternoon vs. late-afternoon), all the other timepoints showed
366 significant differences.
367

368 *Temporal characterization of oyster-microbiomes*

369 The 16S rRNA amplicon sequencing generated a total of 2,032,567 reads from 30
370 samples which were reduced to 1,126,884 after denoising and quality control. These reads were
371 then used to characterize the microbial communities of *I. nucleus* across the different time
372 points. Due to the low sequence counts, samples BRM3 (5612 reads) and DRM4 (7519 reads)
373 were removed after each sample was rarefied to a sampling depth of 21,282 reads.

374 The ASV richness and Shannon-Wiener index of *I. nucleus* were significantly different
375 across the emersion period (Fig. 4; ASV richness: $_{3,14)} = 3.67$; p-value < 0.05; Shannon-Wiener
376 index: $F_{(3,14)} = 3.76$; p-value < 0.05). However, no specific temporal trends were detected for
377 all pairwise comparisons in ASV richness. Significant differences were, however, found for the
378 Shannon-Wiener index between morning and noon timepoints. Oyster body temperature
379 significantly influenced ASV richness and Shannon-Wiener indexes (Fig. S2). Overall,
380 morning timepoints showed the highest alpha diversity. This diversity then drastically declined
381 at noon, with partial recovery at the last timepoint – late-afternoon.

382 The top 10 most abundant microbial taxa (at the family level) associated with *I. nucleus*
383 were *Mycoplasmataceae, Helicobacteraceae, Spirochaetaceae, Xenococcaceae,*
384 *Rhodobacteceae, Rickettsiales* unknown*, Arcobactericeae, Caldilineaceae,*
385 *Alphaproteobacteria* unknown and *Saprospiraceae* (Fig. 5 and 6). These top 10 families made
386 up on average 57.09%, 80.88%, 81.42%, and 68.20% of the overall relative abundance in
387 morning, noon, early-afternoon, and late-afternoon, respectively. Among them, only two
388 families (*Helicobacteraceae* and *Arcobacteraceae*) showed significant differences in the
389 relative abundance between timepoints based on the ANCOM-BC analysis (Fig. 6;
390 *Helicobacteraceae*: morning vs early-afternoon; *Arcobacteraceae*: morning vs noon, and
391 morning vs early-afternoon).

392 No significant difference between timepoints was detected in the taxonomic and
393 functional microbiome structures (Fig. 7, Table 2), but significant differences were detected in
394 their dispersion (Fig. 7, Table 3). Major differences in the microbiome dispersion based on
395 taxonomy were found between morning and early-afternoon, which corresponds to the pre-and

post-noon period, respectively. For the functional microbiome, the pair early-afternoon-late-afternoon was the cause of the difference in dispersion. Despite the changes found in some bacterial taxa and microbiome dispersions, no Mantel correlation was observed between the microbiome taxonomic profile and the PUFA-oxidised metabolite profile, either with the 15 (all) or 4 metabolite groups (Table 4).

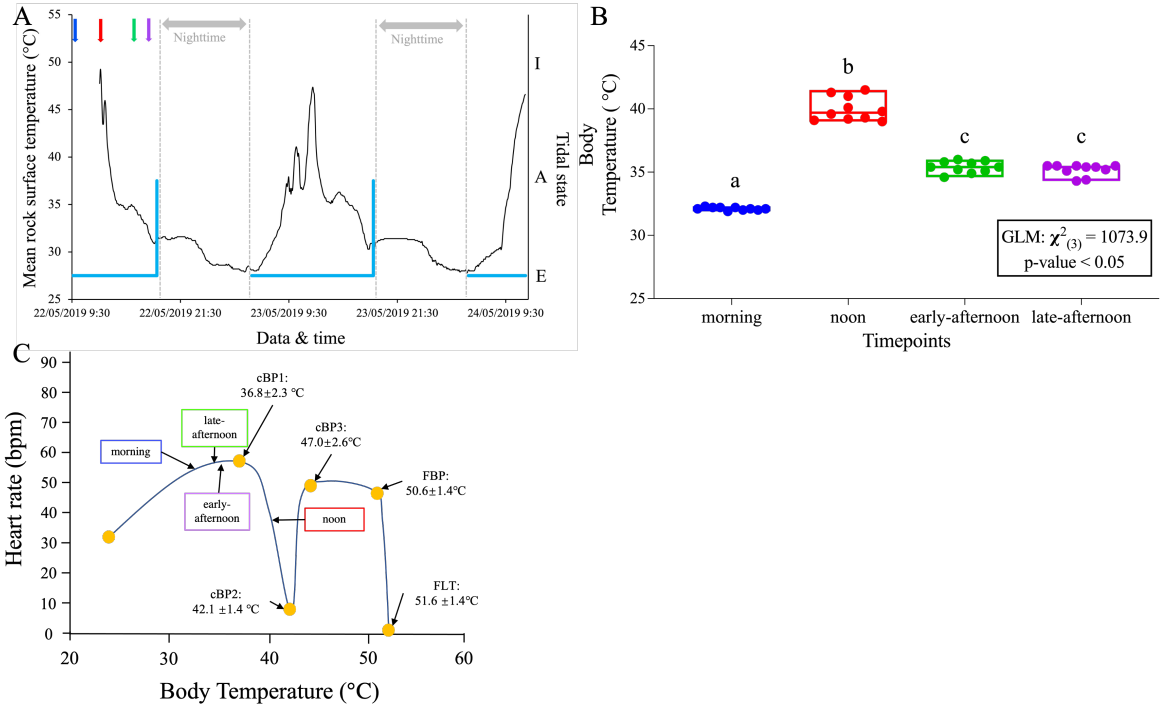

Fig. 1. The body temperature of *Isognomon nucleus* varies across sampling timepoints within a tidal cycle. (A) Thermal (black line) and tidal conditions (blue line) as experienced by *I. nucleus* at the study site. Thermal condition is represented by the mean rock surface temperature (averaged over 3 – 5 i-Button temperature loggers), and tidal condition during the day is categorized into three states: "E" (exposed), "A" (awash), and "I" (immersed). Black arrows indicate the sampling time points of *I. nucleus* to assess its physiological responses (i.e., biochemical dynamics) and microbiome taxonomic/functional profile (B) Boxplots showing *I. nucleus* body temperatures (n=10) across different timepoints (Centre line represent the median; box limits indicate the first and third quartiles). Statistical significance (p-value < 0.05) is indicated if the letters above each bar are different. (C) Schematic diagram of *I. nucleus* cardiac thermal performance curves (TPC) over a gradient of increasing temperature (adapted from Hui et al. (2020)). Coloured text boxes indicated the sampling timepoints (body temperatures) of the *I. nucleus* in the TPC. The abbreviated labels (with temperatures) and arrows pointing to the yellow circles refer to the different critical body temperature for cardiac thermal performances (see Hui et al. (2020); cBP–- critical breakpoints, FBP–- Final breakpoint, FLT Flatline temperature). Metabolic depression breadth is defined as between cBP1 and cBP3.

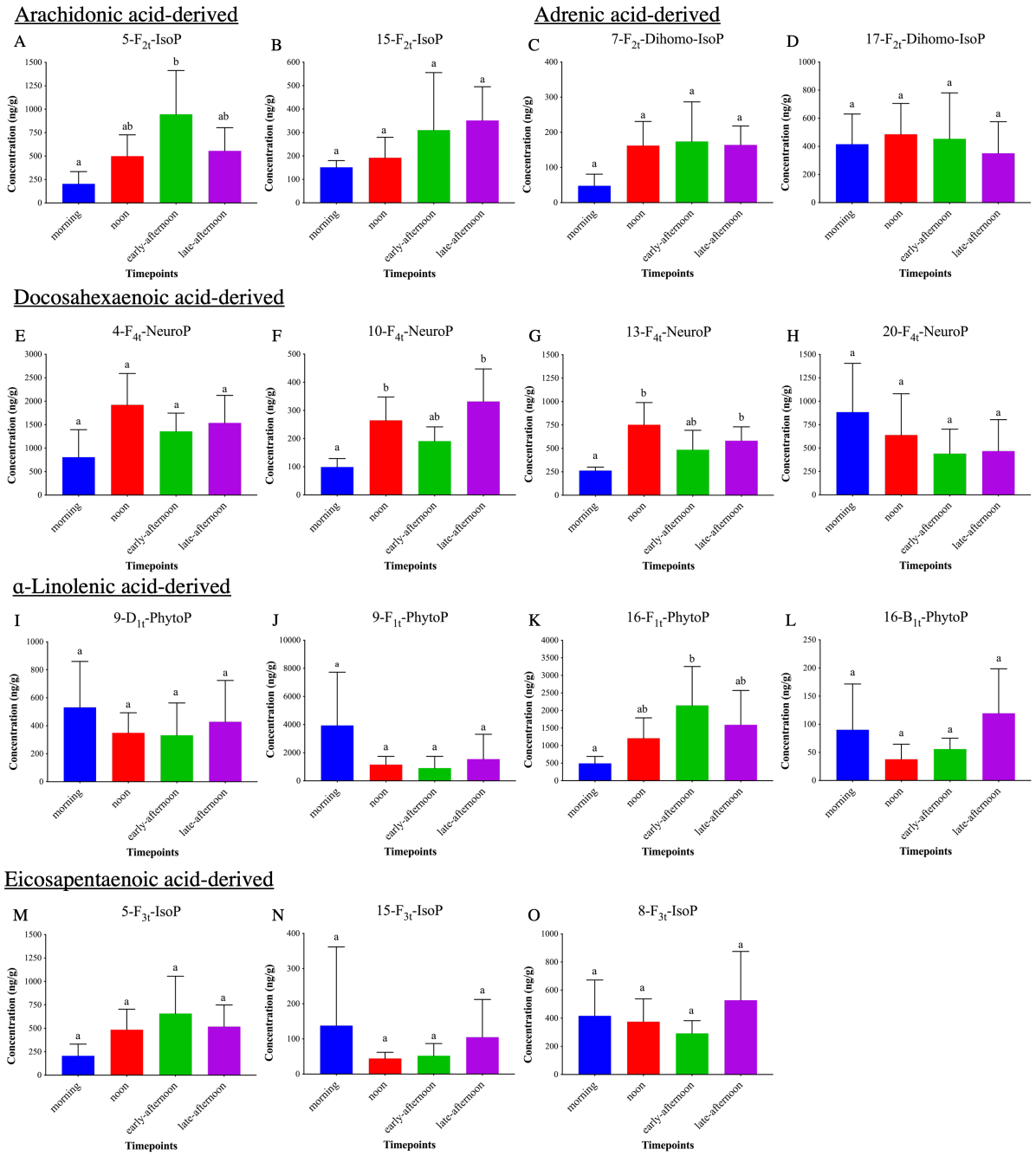

Fig. 2. Four PUFA-oxidised metabolites exhibit variation in concentration across the emersion period. Bar graphs showing the metabolites derived from Arachidonic acid: (A) 5-F_{2t}-IsoP (B) 15-F_{2t}-IsoP; from Adrenic acid: (C) 7-F_{2t}-Dihomo-IsoP (D) 17- F_{2t}-Dihomo-IsoP; from Docosahexaenoic acid: (E) 4-F_{4t}-NeuroP (F) 10-F_{4t}-NeuroP (G) 13-F_{4t}-NeuroP (H) 20-F_{4t}-NeuroP; from α-Linolenic acid: (I) 9-D_{1t}-PhytoP (J) 9-F_{1t}-PhytoP (K) 16-F_{1t}-PhytoP (L) 16-B_{1t}-PhytoP; from Eicosapentaenoic acid: (M) 5-F_{3t}-IsoP (N) 15-F_{3t}-IsoP (O) 8-F_{3t}-IsoP, across different sampling timepoints in *I. nucleus*. IsoP: isoprostane; NeuroP: neuroprostane; PhytoP: phytoprostanes. Data are presented as mean concentration and + 1 standard deviation (error bar) for each metabolite (n=5) at the given timepoints. Statistical significance (p-value < 0.05) is indicated if the letters above each bar are different.

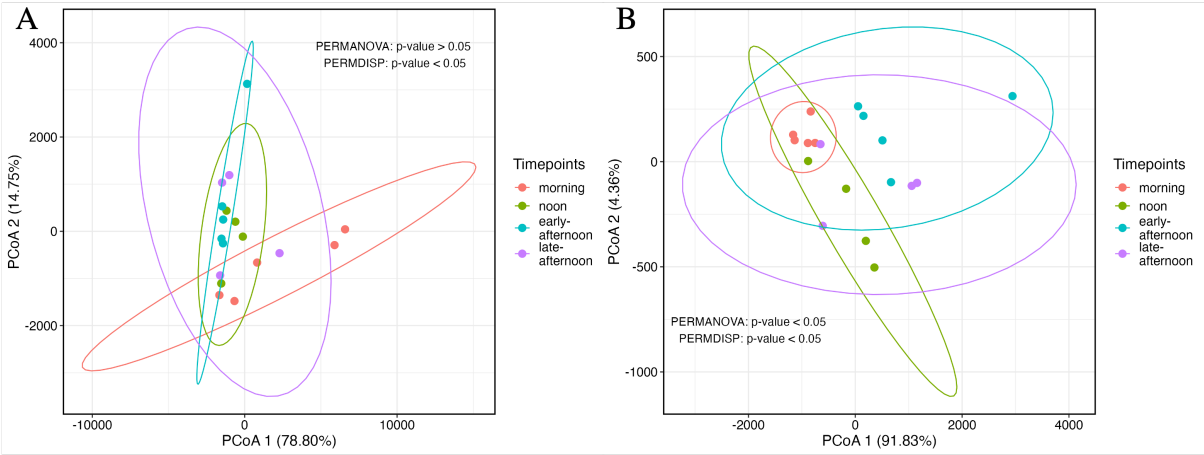

Fig. 3. Four PUFA-oxidised metabolites drive variation in the sample clusters across the emersion period. PCoA based on Euclidean distance measured between samples from different timepoints based on (A) all PUFA-oxidised metabolites (B) four PUFA-oxidised metabolites: 5-F_{2t}-IsoP, 10-F_{4t}-NeuroP, 13-F_{4t}-NeuroP, and 16-F_{1t}-PhytoP. The colours of the datapoints and ellipses (95% confidence interval of the true multivariate means) indicate their corresponding timepoints.

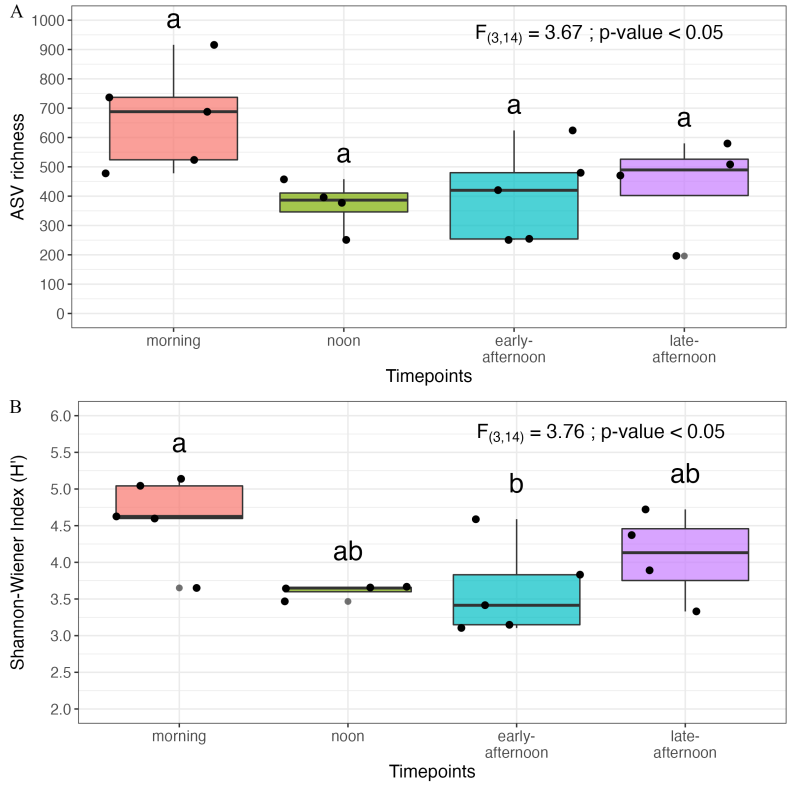

Fig. 4. *I. nucleus*-associated microbiome ASV richness and Shannon-Wiener diversity across the emersion period. Boxplot showing the alpha diversity index of (A) ASV richness, and (B) Shannon-Wiener index (H') of the oyster-associated microbiome at different timepoints. (Centre line represents the median; box limits indicate the first and third quartiles; the lower and upper whiskers indicate the smallest and largest values that within 1.5 times of the IQR (Inter-quartile range) from the first and third quartiles, respectively. The data points shown in each timepoint is replicate values. Statistical significance ($p < 0.05$) is indicated if the letters above each boxplot are different between any two timepoints.

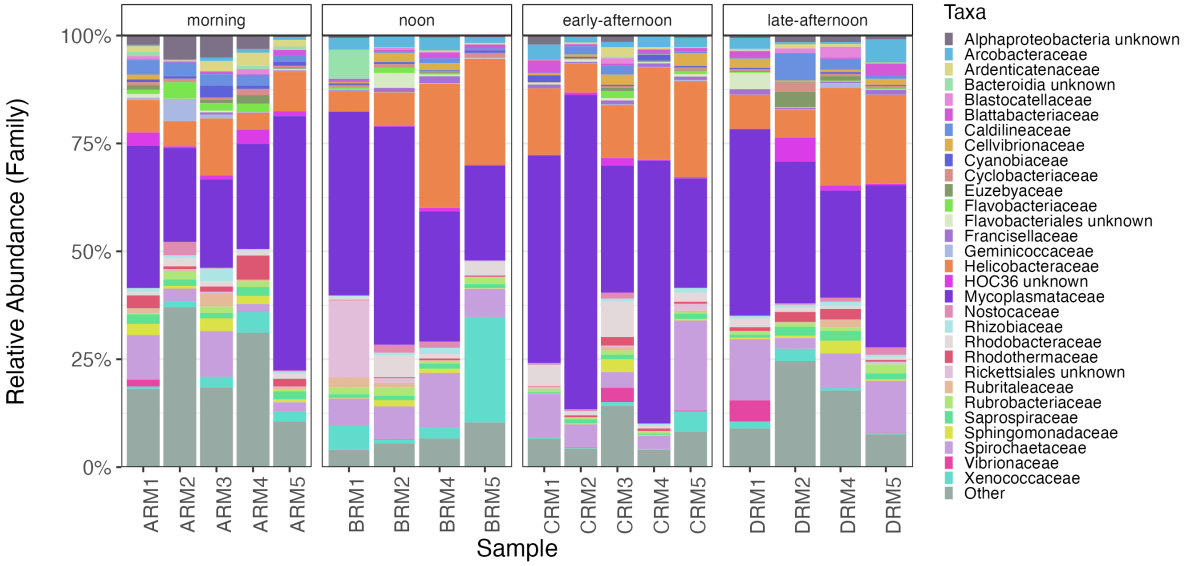

Fig. 5. Relative abundance of top 30 most dominant microbial taxa associated with the *I. nucleus's* gut microbiome at each sampling timepoints. ASV counts were aggregated into the family taxonomic level. Each bar represents a single individual replicate of oyster gut microbiome.

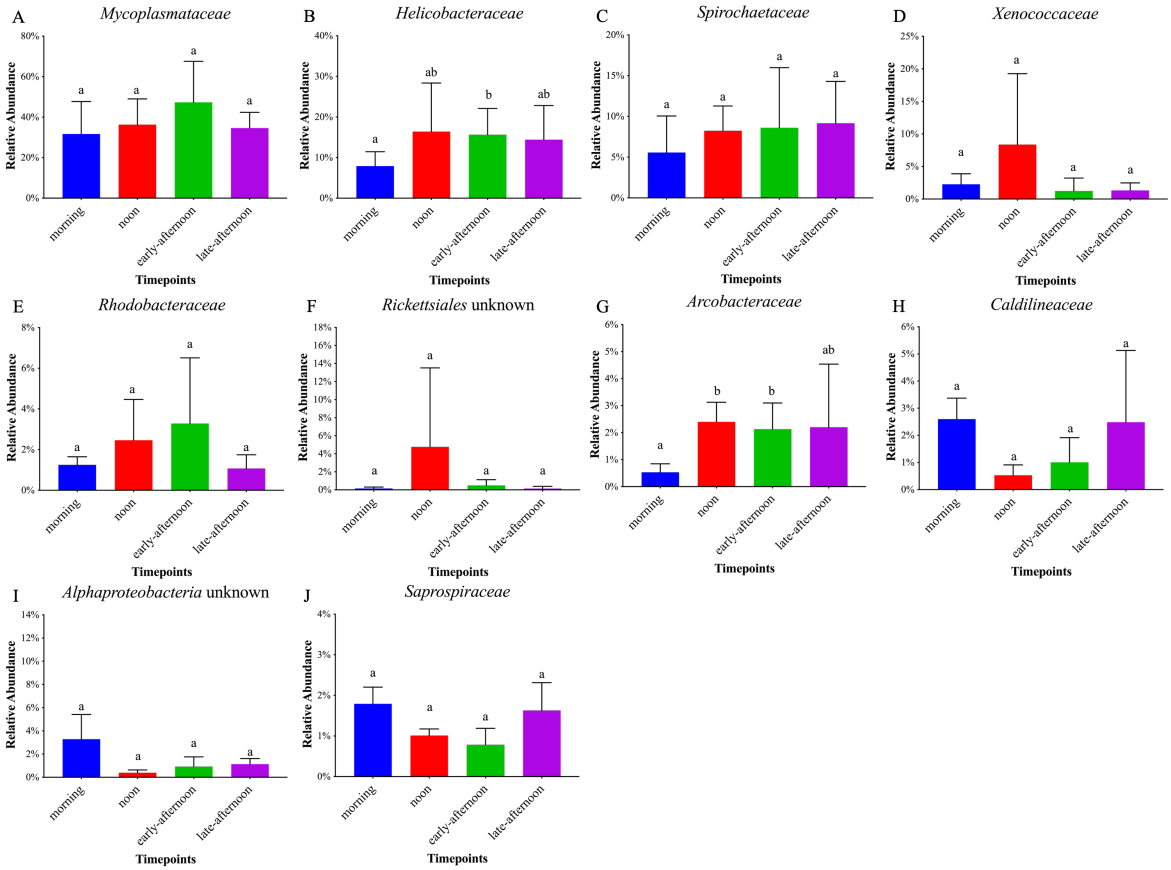

Fig. 6. *Helicobacteraceae* and *Arcobacteraceae* mean relative abundance vary across the emersion period. Bar graphs showing the top 10 dominant family level taxa in *I. nucleus*'s gut microbiome at each timepoint: (A) *Mycoplasmataceae* (B) *Helicobacteraceae* (C) *Spirochataceae* (D) *Xenococcaceae* (E) *Rhodobacteraceae* (F) *Rickettsiales* unknown (G) *Arcobacteraceae* (H) *Caldilineaceae* (I) *Alphaproteobacteria* unknown (J) *Saprospiraceae*. For F and I, the taxa were assigned with the lowest taxonomic level name identifiable. Data are

presented as mean relative abundance and + 1 standard deviation (error bar) for each taxon at the given timepoints. Statistical significance (p-value < 0.05) is indicated if the letters above each bar are different.

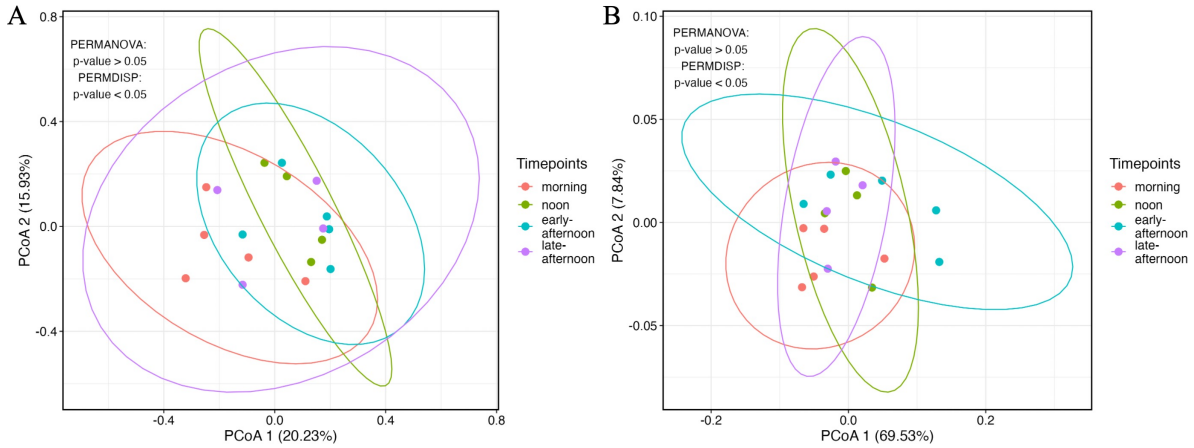

Fig. 7. *I. nucleus*-associated microbiome taxonomic and functional structures exhibit overall stability across the emersion period. PCoA based on the Bray-Curtis distance metric measured between samples from different timepoints, based on (A) taxonomy (ASV level) and (B) functions (MetaCyc pathways). The colours of the datapoints and ellipses (95% confidence interval of the true multivariate means) indicate their corresponding timepoints.

Table 1. Statistical analysis result (ANOVA or GLM with gamma distribution) testing the effect of timepoints on the concentration of each of the PUFA-oxidised metabolites.

PUFA	Metabolite	Test Statistic	p-value
Arachidonic acid	5-F_{2t}-IsoP	$F_{(3,14)} = 5.08$	**< 0.05**
	15-F_{2t}-IsoP	$F_{(3,14)} = 1.72$	> 0.05
Adrenic acid	7-F_{2t}-Dihomo-IsoP	$F_{(3,14)} = 3.10$	> 0.05
	17-F_{2t}-Dihomo-IsoP	GLM $\mathcal{X}^2_{(3)} = 0.66$	> 0.05
Docosahexaenoic acid	4-F_{4t}-NeuroP	$F_{(3,14)} = 3.13$	> 0.05
	10-F_{4t}-NeuroP	$F_{(3,14)} = 8.43$	**< 0.05**
	13-F_{4t}-NeuroP	GLM $\mathcal{X}^2_{(3)} = 27.46$	**< 0.05**
	20-F_{4t}-NeuroP	$F_{(3,14)} = 1.23$	> 0.05
α-Linolenic acid	9-D_{1t}-PhytoP	$F_{(3,14)} = 0.58$	> 0.05
	9-F_{1t}-PhytoP	GLM $\mathcal{X}^2_{(3)} = 7.92$	> 0.05
	16-F_{1t}-PhytoP	$F_{(3,14)} = 3.72$	**< 0.05**
	16-B_{1t}-PhytoP	GLM $\mathcal{X}^2_{(3)} = 6.66$	> 0.05
Eicosapentaenoic acid	5-F_{3t}-IsoP	$F_{(3,14)} = 2.49$	> 0.05
	15-F_{3t}-IsoP	GLM $\mathcal{X}^2_{(3)} = 0.32$	> 0.05
	8-F_{3t}-IsoP	$F_{(3,14)} = 0.81$	> 0.05

474
475 **Table 2.** Permutation multivariate analysis of variance (PERMANOVA) to investigate
476 differences in the PUFA-oxidised metabolites or microbiome structure in taxonomy/functions
477 across the emersion period. The number of permutations performed was 999 times. The
478 numerator and denominator degree of freedom were 3 and 14, respectively.

Category	Distance metric	*pseudo-F*	R^2	p-value
PUFA-oxidised metabolites (all)	Euclidean	2.14	0.31	> 0.05
PUFA-oxidised metabolites (four)*	Euclidean	4.02	0.46	**< 0.05**
Microbiome (Taxonomy)	Bray-Curtis	1.18	0.20	> 0.05
Microbiome (Function)	Bray-Curtis	1.49	0.24	> 0.05

479 *The four metabolites were: 5-F_{2t}-IsoP, 10-F_{4t}-NeuroP, 13-F_{4t}-NeuroP, and 16-F_{1t}-PhytoP
480
481 **Table** 3. Permutational analysis of multivariate dispersions (PERMDISP) analysis to
482 investigate differences in the PUFA-oxidised metabolites or microbiome structure in
483 taxonomy/functions across the emersion period. The number of permutations performed was
484 999 times.

Category	Distance metric	F-value	p-value
PUFA-oxidised metabolites (all)	Euclidean	6.88	**< 0.05**
PUFA-oxidised metabolites (four)*	Euclidean	3.51	**< 0.05**
Microbiome (Taxonomy)	Bray-Curtis	3.55	**< 0.05**
Microbiome (Functions)	Bray-Curtis	3.74	**< 0.05**

485 *The four metabolites were: 5-F_{2t}-IsoP, 10-F_{4t}-NeuroP, 13-F_{4t}-NeuroP, and 16-F_{1t}-PhytoP
486
487

Table 4. Mantel's spearman's rank correlation (r) and p-value to investigate the association between the *I. nucleus* microbiome taxonomic structure (mean abundance of each taxon across all timepoints) and PUFA-oxidised metabolite profile (mean concentration across timepoints). The number of permutations performed was 23(maximum possible).

Association with microbiome taxonomic structure	Mantel's r	p-value
PUFA-oxidised metabolites (all)	0.7134	> 0.05
PUFA-oxidised metabolites (Four)*	0.1343	> 0.05

*The four metabolites were: 5-F_{2t}-IsoP, 10-F_{4t}-NeuroP, 13-F_{4t}-NeuroP, and 16-F_{1t}-PhytoP

Discussion

Organisms living on the intertidal rocky shore regularly experience drastic changes in environmental temperature (Harley, 2008; Somero, 2002; Stillman, 2002). For many sessile ectotherms, this represents a physiological challenge due to their inability to escape from heat stress (e.g. seeking thermal refuge) and so, they rely on various intrinsic (metabolic and physiological plasticity) and extrinsic (host-associated microbiome) mechanisms to cope with temperature fluctuations (Bang et al., 2018; Giomi et al., 2016; Huang et al., 2020; Lathlean et al., 2014). As with other ectotherms, the body temperature of the high shore oyster, *Isognomon nucleus* was highly influenced by changes in ambient temperatures throughout the day. Such changes are known to induce physiological stress and metabolic depression (Hui et al., 2020), with the associated oxidative stress (Hermes-Lima et al., 2015). Here, linked to these physiological conditions, we found adjustments in four major non-enzymatic PUFA-oxidised metabolites (i.e., 5-F_{2t}-IsoP, 10-F_{4t}-NeuroP, 13-F_{4t}-NeuroP, and 16-F_{1t}-PhytoP) that reflect temporal variation in the oxidative stress experienced by the oysters. Contrary, no clear temporal extrinsic adjustments in the structure and/or function of the gut microbiome were detected despite the temporal changes in environmental conditions. This suggests that the oyster gut microbiome is temporally stable and insensitive to extreme thermal conditions (> 40ºC in body temperature) that are physiologically stressful to the oyster host. The differences in the host and microbiome sensitivity to external changes was further supported in the lack of temporal correlation between the intrinsic (biochemical profile) and extrinsic (microbiome taxonomic structure) mechanisms. In summary, the microbiome stability may be important for the overall homeostasis of the oysters, contributing to their thermal tolerance and survival in the challenging tropical intertidal rocky environment.

518 *The intrinsic mechanism underpinning oysters' adaptive response to temporal*
519 *environmental changes*

520 For high-shore intertidal ectotherms, metabolic depression is an adaptive response that
521 allows them to cope with extreme and stressful thermal conditions (Hui et al., 2020; Marshall
522 et al., 2011; Sokolova and Pörtner, 2001). This physiological adjustment is a common signal
523 that the animal is under thermal stress and acts as a strategy to conserve energy required for
524 critical functions during normal metabolic resumption (i.e., less stressful thermal conditions;
525 Hand and Hardewig, 1996; Marshall and McQuaid, 2020). Metabolic depression is also known
526 to be an important mechanism to reduce/avoid the over-production of harmful ROS that results
527 from the rapid increase in metabolic demands under elevated temperatures (Abele et al., 2002;
528 Storey and Storey, 2004). Hui et al. (2020) demonstrated that the oyster *I. nucleus* consistently
529 enters into metabolic depression when body temperature approaches ~ 37°C (a value that is
530 regularly surpassed on daily basis at around noon on tropical rocky shores). This suggests that
531 these animals should enter a state of metabolic depression when exposed by the tide during
532 noon time and resume their metabolism when body temperatures lower in late
533 afternoon/evening, or when they are re-immersed. During the low tide, oysters are exposed to
534 anaerobic conditions because of the closure of the shell, which prevents oxygen exchange with
535 the environment (Chapman et al., 2011). However, as with other intertidal bivalves, oysters can
536 display intermittent gaping behaviour during periods of aerial exposure as a way to enhance
537 oxygen intake and evaporative cooling, particularly when experiencing thermal stress (Lent,
538 1969; Mcmahon, 1988; Nicastro et al., 2010). In our study, all individuals shut their valves and
539 no intermittent gaping behaviour was observed either during the high thermal stress or the
540 recovering period (Hui, T.Y., unpublished data). Therefore, oxygen depletion is a plausible
541 stress in the oysters particularly under elevated body temperatures as experienced during noon
542 time, and anaerobic respiration is likely to contribute to the oysters' metabolic demand during
543 such thermally stressful conditions.

544 As part of the metabolic depression, intertidal ectotherms modulate biochemical
545 molecules such as polyunsaturated fatty acids (PUFA) to cope with the elevated thermal and
546 oxidative stress conditions in their environment (Dubousquet et al., 2016; Pernet et al., 2008).
547 The higher metabolic demand driven by higher temperatures generate ROS during and after
548 thermal stress and/or under hypoxia (Byrne et al., 1990; Freire et al., 2011; Rivera-Ingraham et
549 al., 2013; Welker et al., 2013). PUFAs such as ARA, DHA, and EPA are known to be effective
550 molecules to mitigate the effect of ROS (Lund and Steenfeldt, 2011; Yin et al., 2017). This is

because these PUFA contain unsaturated double bonds making them susceptible to ROS reaction (particularly to peroxide, HO•), and thus could be an agent for ROS removal (Fadhlaoui and Lavoie, 2021; Leung et al., 2015; Sargent, 1976). The non-enzymatic peroxidation of these PUFAs, therefore, generates by-products that can be used as biomarkers of the ROS level (Galano et al., 2017; Miller et al., 2014; Yonny et al., 2016). Using this as a measure of the oyster's biochemical response to thermal environmental changes, we found that there were four metabolites (i.e., 5-F_{2t}-IsoP (Isoprostane), 10-F_{4t}-NeuroP (Neuroprostane), 13-F_{4t}-NeuroP (Neuroprostane), and 16-F_{1t}-PhytoP (Phytoprostane)) that showed visible temporal patterns. Such patterns may be linked to the sensitivity of the metabolites to ROS changes in the oyster. Elevation of 5-F_{2t}-IsoP, 10-F_{4t}-NeuroP, and 13-F_{4t}-NeuroP during noon, and 16-F_{1t}-PhytoP at post-noon timepoints, clearly indicates that oysters experienced a rise in the ROS level, a signal of oxidative stress (Galano et al., 2017; Hermes-Lima and Zenteno-Savín, 2002; Storey and Storey, 2004; Sussarellu et al., 2012; Welker et al., 2013). This could be caused by an increase in metabolic demand and/or hypoxia (when individuals shut their valves and show no gaping behaviour). ALA and its non-enzymatic oxidised by-products (phytoprostanes) are known to be the major molecules to cope with oxidative stress in plants (Durand et al., 2009; Imbusch and Mueller, 2000; Jahn et al., 2008; Loeffler et al., 2005; Thoma et al., 2003). For filter-feeding bivalves, ALA can be obtained from phytoplankton, which is a major part of their diet (Sargent, 1976; Zhukova, 2019). In our study, the high levels of 16-F_{1t}-PhytoP (Phytoprostane) metabolites as compared to other three PUFA-oxidised metabolites in the *I. nucleus,* imply that the PUFA ALA could also be the predominant fatty acid in alleviating oxidative stress in this oyster. Thus, for *I. nucleus,* phytoplankton, through their fatty acid composition, are likely to provide key benefits for their physiological regulation and survival in the thermally and oxidatively stressful conditions at the high shore environment.

The structural profile of the ROS-sensitive metabolites exhibits clear temporal variation and inter-individual variation in the *I. nucleus*. The large inter-individual variability in the PUFA-metabolites profile at noon/afternoon relative to morning timepoint might be related to the thermal and oxidative stress conditions experienced by the oysters during those periods of elevated temperatures. This variability suggests inter-individual differences in physiological plasticity, regulation, and sensitivities to environmental stress. The result here also indicates that the polyunsaturated fatty acids (ARA, DHA, and ALA) from which these four PUFA-oxidised metabolites were derived, may play a key role acting as 'resolving' lipid mediators needed by the oysters to return to homeostasis (Lee et al., 2020; Roy et al., 2017).

584 *The extrinsic mechanism underpinning the oysters' adaptive response to*
585 *temporal environmental changes*

586 Host-associated microbiome diversity, structure, and functions are more frequently
587 considered as important components of animal adaptation and acclimation to environmental
588 change (Bang et al., 2018; Foster et al., 2017; Voolstra and Ziegler, 2020). Alterations in
589 microbiome diversity can be associated with the direct influence of the host's physiology and/or
590 with host-independent environmental effects (Li et al., 2018; Li et al., 2022; Muñoz et al., 2019;
591 Shiu et al., 2017). In our study, the composition and diversity (ASV richness and Shannon
592 diversity) of the oyster gut-associated microbiome varied with time which coincided with
593 variation in the oyster's body temperature, suggesting that the thermal condition experienced
594 by the host may modulate the microbial alpha diversity via either direct/indirect physio-
595 biochemical influences (Apprill, 2017; Pita et al., 2018; Sorek et al., 2014). In the morning, the
596 oyster's gut had a significantly more diverse microbiome diversity, which may be linked to the
597 less thermally stressed host (Hui et al., 2020), and/or to the filter-feeding activities before being
598 exposed by the receding tide (Parris et al., 2019). However, at noon, a major decline in diversity
599 was observed, which may be associated with the thermal physiological stress experienced by
600 the host (body temperature is within the metabolic depression range; Hui et al., 2020) and
601 oxidative stress (indicated by the rise in the PUFA-oxidised metabolites). This decline in
602 diversity is also a common pattern seen in many marine organisms under physiological stress
603 (Green and Barnes, 2010; Hartman et al., 2020; Li et al., 2018). For example, Lokmer &
604 Wegner (2015) showed that thermal stress and/or infection caused a marked decline in the alpha
605 diversity of the microbiome in the oyster *Crassostrea gigas*. Interestingly, in our study, during
606 the late afternoon timepoint, we observed an increase in the microbiome diversity, driven by an
607 increase in the extremely low abundant taxa, most of them undetectable at noon. This trend
608 suggests that the stress condition experienced during the day did not cause an irreversible
609 breakdown in the host-microbiome relationship, in which diversity seems resilient probably as
610 a consequence of the predictability and magnitude of the environmental change (Huus and Ley,
611 2021; Longford et al., 2019; Narrowe et al., 2015; Webster et al., 2008). It is unclear, however,
612 whether this trend would be maintained when stressful conditions are extreme and
613 unpredictable, such as in the case of marine heatwaves.

614 Whilst the temporal changes exhibited by the *I. nucleus* microbiome and their
615 association with changes in the oysters' body temperatures suggest that the microbiome
616 composition may be actively regulated by the host, differential sensitivities of certain bacterial

taxa to external environmental changes may also be an important mechanism driving the temporal variation in the microbiome composition. *Helicobacteraceae* and *Arcobacteraceae* are the only two dominant family-level microbial taxa associated with the temporal thermal/oxidative stress variation of the host. In particular, there was an elevated relative abundance of these two bacteria groups at noon and/or at the afternoon timepoints, which may suggest that their abundances during these periods were promoted by specific host/environmental conditions, facilitating their growth probably by reducing competition (Garren et al., 2016; Sharp and Foster, 2022; Shaver et al., 2017). *Arcobacteraceae* is a group of common opportunistic bacteria found in marine bivalves and is known to be associated with disease-causing bacteria such as *Vibrio* (de Lorgeril et al., 2018; Lokmer and Mathias Wegner, 2015). In many studies, the elevation of the *Arcobacteraceae* has been associated with the thermal stress condition experienced by the host (Lokmer and Mathias Wegner, 2015; Neu et al., 2021; Shiu et al., 2017). Members of *Arcobacteraceae* are also known to be microaerophilic as they tend to grow better under a low-oxygen environment (Vandamme and De Ley, 1991). This may explain the dominant presence of *Arcobacteraceae* within the oysters' microbiome due to the prevailing hypoxic and thermally stressful conditions as experienced by the oyster hosts during emersion. Similarly, the presence and abundance *Helicobacteraceae* can be associated to oxygen levels in the marine environment. For instance, certain members of this family are capable of oxidising sulfide, and thus, they might contribute with a detoxification function to the oyster host (Kodama and Watanabe, 2004; Nakagawa et al., 2017; Neu et al., 2021). The accumulation of sulfide can be detrimental or lethal to marine bivalves (Le Moullac et al., 2008), and it is typically associated with hypoxic stress (Le Moullac et al., 2008; Pal et al., 2018). Such stress is hypothesised to occur in *I. nucleus* during aerial exposure, as no intermittent gaping behaviour was detected. When oxygen is low, sulfide production is promoted by the activity of hydrogen sulfide-producing bacteria such as *Desulfobacterota* members (present in the *I. nucleus*; Dordević et al., 2021; Flannigan et al., 2011; Pimentel et al., 2021). It is unclear, however, the extent to which the dynamics in the abundance of sulfide-producing bacteria and *Helicobacteraceae* members (with potential detoxification role), are functionally interconnected. While this seems likely, we are unaware of any study exploring this functional link, and it would be important to investigate such species' interaction and its effects on the physiology and fitness of the host.

Host tolerance and resilience to environmental stress are known to be conditioned by the stability/flexibility of its associated microbiome. Despite the changes in the alpha diversity and relative abundance of some of the most abundant bacteria (family level) in *I. nucleus*, the

651 structural and functional microbiome profiles showed an overall stability throughout the day
652 (emersion period). Such stability could be potentially explained by the ability of the host to
653 control/regulate the microbiome during a disturbance event (Pita et al., 2018; Rädecker et al.,
654 2022; Rocca et al., 2019; Sharp et al., 2017). Alternatively, the stability of the microbiome may
655 reflect its own resilience (or lower sensitivity), rather than the host control/regulation, to
656 changing and stressful environments (Soen, 2014). This characteristic could be essential for
657 host tolerance and acclimation to environmental challenges such as thermal stress. For example,
658 Santoro et al. (2021) demonstrated that the stability of inoculated "beneficial microorganisms"
659 in the coral *Mussismilia hispida* provided a thermal protection effect, reducing heat stress and
660 preventing the associated mortality (40% increase in the survival rate) of the hosts. Contrary,
661 disruptions in the microbiome structure and function can lead to a weakened thermal tolerance
662 and performance of the host, and a decrease in survival rate under prolonged heat stress
663 condition, particularly in early ontogenetic stages such as in the tadpoles of the green frog
664 *Lithobates clamitans* (Fontaine et al., 2022). Overall, regardless of the mechanisms, the
665 temporal stability in the microbiome structure and function found in this study may imply a
666 fundamental ecological role for *I. nucleus* survival in the thermally extreme tropical intertidal
667 environment (Bang et al., 2018).
668

669 *No correlation between microbiome structure and PUFA-oxidised metabolite*
670 *profile*

671 Over the decades, many studies have documented the role and action of PUFA (e.g., as
672 probiotics) in modulating dynamics in the gut microbiome of different animals (Fu et al., 2021;
673 Huyben et al., 2020; Lau et al., 2022; Ma et al., 2022). Hence, it is expected that stress-driven
674 changes in these biochemicals and their by-products would influence the oyster gut microbiome.
675 However, we found no correlation between the PUFA-oxidised metabolites and microbiome
676 taxonomic structure in *I. nucleus*, despite the temporal and inter-individual variation in the
677 PUFA-oxidised metabolite profile across the emersion period. The lack of association between
678 the microbial and PUFA-oxidised metabolites profiles of *I. nucleus*, suggests two possibilities
679 that are not mutually exclusive. Firstly, as mentioned previously, physiological/biochemical
680 and microbiome profiles may have different sensitivities to changes in environmental
681 conditions. Secondly, such microbiome profiles and biochemical responses may not show
682 strong variation and/or alignment because of local adaptation. Here, the thermal window and
683 oxygen levels experienced by the oysters, although extreme for many ectotherms, can be

684 considered within the tolerance range of the species. Several studies have shown that the
685 microbiome-metabolites correlation is detectable only under severe post-disturbance events and
686 unhealthy host conditions (Mallott et al., 2022; Nguyen et al., 2021; Paix et al., 2019; Pimentel
687 et al., 2021; Shankar et al., 2015; Walke et al., 2021), which go beyond tolerance levels. Thus,
688 in this study, oysters may be in a condition where stress is within the tolerance range, and thus
689 no correlation can be observed between these two components (i.e., host biochemical profile
690 and microbiome structure). Future studies aiming to explore the functional regulation and
691 interplay between intrinsic and extrinsic mechanisms in ectotherms living in extreme
692 environments require the assessment of both components when animals are closer to or surpass
693 their physiological tolerance limits at sublethal levels.
694

695 # Conclusion

696 Intrinsic (e.g., non-enzymatic PUFA-oxidised metabolites) and extrinsic (e.g.,
697 microbiome profile) mechanisms linked to the ecophysiology and tolerance/sensitivity of the
698 oyster *Isognomon nucleus*, showed temporal variation indicative of thermal and oxidative stress.
699 Such trend was tightly aligned to changes in environmental and body temperatures during the
700 tidal cycle where oysters were fully emersed. Although the microbial alpha diversity in the
701 oyster gut varied along this temporal and environmental cycle, no major changes were detected
702 in the overall structure and function of the associated microbial communities. This microbiome
703 stability along periods of extreme temperature and oxygen deprivation, could be explained by
704 the potential regulatory influence of the host (consistent with the Anna Karenina Principle)
705 and/or the insensitivity of these microorganisms to the environmental changes experienced in
706 the tropical rocky shores. When assessing both the intrinsic and extrinsic mechanisms together,
707 we found no clear correlation between the PUFA-oxidised metabolites profile and the
708 microbiome profile. However, some specific bacteria groups (i.e., *Helicobacteraceae* and
709 *Arcobacteraceae*) increased during stressful periods, potentially linked to the lower oxygen
710 availability within the oysters due to the lack of gaping behaviour when emersed. These
711 microorganisms may provide important functions for the resilience and stability of the overall
712 microbial community, as well as for the health and survival of the oyster host in the thermally
713 challenging rocky intertidal environment. The overall microbiome stability can avoid dysbiosis
714 and contribute to the intrinsic adaptive adjustment of oyster physiology and biochemistry. To
715 our best knowledge, this is the first study to report the use of non-enzymatic PUFA-oxidised
716 metabolites as a proxy for oxidative stress levels in intertidal animals and profiling short-term

dynamics of the host-associated microbiome in an intertidal environment. Future investigations should aim to explore the interplay between these biomolecules and microbial patterns when stressful environmental conditions are unpredictable and beyond tolerance windows of the hosts. Moreover, it is important to understand whether these functional links between intrinsic and extrinsic mechanisms are modulated by local adaptation and can be shared among other intertidal organisms.

Competing interests

The authors declare no competing or financial interests

Author Contributions

JDGE and BSA conceived the idea and designed the work. BSA carried out most of the work: data collection, sample processing, statistical analyses, and data presentation. AWTC, HTY GAW, and MG were involved in sample and environmental data collection. LKS performed the PUFA-oxidised metabolites extraction and processing. TD supplied the in-house synthesised oxidised lipids standards for PUFA metabolites quantification. JTY and TD were involved in analysing the metabolite data. BSA led the manuscript writing with feedback and input from all authors.

Acknowledgement

We would like to thank The Swire Group of Companies, especially Ms. Tina Chan and Cathay Pacific staff for arranging air transportation of equipment to and from Thailand from Hong Kong

Funding

JDGE was supported by the Research Grants Council (ECS 27124318) of Hong Kong.

Data availability

All raw data, and scripts will be made available once published.

References

Abele, D., Heise, K., Pörtner, H. O. and Puntarulo, S. (2002). Temperature-dependence of mitochondrial function and production of reactive oxygen species in the intertidal mud clam Mya arenaria. *J. Exp. Biol.* **205**, 1831–1841.

Ahmed, H. I., Herrera, M., Liew, Y. J. and Aranda, M. (2019). Long-term temperature stress in the Coral Model Aiptasia supports the "anna Karenina principle" for bacterial microbiomes. *Front. Microbiol.* **10**, 975.

Alberdi, A., Aizpurua, O., Bohmann, K., Zepeda-Mendoza, M. L. and Gilbert, M. T. P. (2016). Do Vertebrate Gut Metagenomes Confer Rapid Ecological Adaptation? *Trends Ecol. Evol.* **31**, 689–699.

Apprill, A. (2017). Marine animal microbiomes: Toward understanding host-microbiome interactions in a changing ocean. *Front. Mar. Sci.* **4**, 222.

Bäckhed, F., Roswall, J., Peng, Y., Feng, Q., Jia, H., Kovatcheva-Datchary, P., Li, Y., Xia, Y., Xie, H., Zhong, H., et al. (2015). Dynamics and stabilization of the human gut microbiome during the first year of life. *Cell Host Microbe* **17**, 690–703.

Bang, C., Dagan, T., Deines, P., Dubilier, N., Duschl, W. J., Fraune, S., Hentschel, U., Hirt, H., Hülter, N., Lachnit, T., et al. (2018). Metaorganisms in extreme environments: do microbes play a role in organismal adaptation? *Zoology* **127**, 1–19.

Basu, S. (2010). Fatty acid oxidation and isoprostanes: Oxidative strain and oxidative stress. *Prostaglandins Leukot. Essent. Fat. Acids* **82**, 219–225.

Birben, E., Sahiner, U. M., Sackesen, C., Erzurum, S. and Kalayci, O. (2012). Oxidative stress and antioxidant defense. *World Allergy Organ. J.* **5**, 9–19.

Bolyen, E., Rideout, J. R., Dillon, M. R., Bokulich, N. A., Abnet, C. C., Al-Ghalith, G. A., Alexander, H., Alm, E. J., Arumugam, M., Asnicar, F., et al. (2019). Reproducible, interactive, scalable and extensible microbiome data science using QIIME 2. *Nat. Biotechnol.* **37**, 852–857.

Byrne, R. A., Gnaiger, E., McMahon, R. F. and Dietz, T. H. (1990). Behavioral and metabolic responses to emersion and subsequent reimmersion in the freshwater bivalve, Corbicula fluminea. *Biol. Bull.* **178**, 251–259.

Callahan, B. J., McMurdie, P. J., Rosen, M. J., Han, A. W., Johnson, A. J. A. and Holmes, S. P. (2016). DADA2: High-resolution sample inference from Illumina amplicon data. *Nat. Methods* **13**, 581–583.

Callahan, B. J., McMurdie, P. J. and Holmes, S. P. (2017). Exact sequence variants should replace operational taxonomic units in marker-gene data analysis. *ISME J.* **11**, 2639–2643.

Carey, H. V. and Duddleston, K. N. (2014). Animal-microbial symbioses in changing environments. *J. Therm. Biol.* **44**, 78–84.

Chapman, R. W., Mancia, A., Beal, M., Veloso, A., Rathburn, C., Blair, A., Holland, A. F., Warr, G. W., Didinato, G., Sokolova, I. M., et al. (2011). The transcriptomic responses of the eastern oyster, Crassostrea virginica, to environmental conditions. *Mol. Ecol.* **20**, 1431–1449.

Chow, C. Y. (2004). Foraging behaviour of Thais clavigera: The interplay of environmental variation and predator behaviour on sheltered rocky shores.

de Lorgeril, J., Lucasson, A., Petton, B., Toulza, E., Montagnani, C., Clerissi, C., Vidal-Dupiol, J., Chaparro, C., Galinier, R., Escoubas, J. M., et al. (2018). Immune-suppression by OsHV-1 viral infection causes fatal bacteraemia in Pacific oysters. *Nat. Commun.* **9**,.

Díaz-almeyda, E. M., Ryba, T., Ohdera, A. H., Collins, S. M., Shafer, N., Link, C., Prado-zapata, M., Ruhnke, C., Moore, M., Angel, A. M. G., et al. (2022). Thermal

Stress Has Minimal Effects on Bacterial Communities of Thermotolerant Symbiodinium Cultures. *Front. Ecol. Evol.* **10**, 764086.

Dordević, D., Jančíková, S., Vítězová, M. and Kushkevych, I. (2021). Hydrogen sulfide toxicity in the gut environment: Meta-analysis of sulfate-reducing and lactic acid bacteria in inflammatory processes. *J. Adv. Res.* **27**, 55–69.

Douglas, G. M., Maffei, V. J., Zaneveld, J. R., Yurgel, S. N., Brown, J. R., Taylor, C. M., Huttenhower, C. and Langille, M. G. I. (2020). PICRUSt2 for prediction of metagenome functions. *Nat. Biotechnol.* **38**, 669–673.

Dubousquet, V., Gros, E., Berteaux-Lecellier, V., Viguier, B., Raharivelomanana, P., Bertrand, C. and Lecellier, G. J. (2016). Changes in fatty acid composition in the giant clam Tridacna maxima in response to thermal stress. *Biol. Open* **5**, 1400–1407.

Dupuy, A., Le Faouder, P., Vigor, C., Oger, C., Galano, J. M., Dray, C., Lee, J. C. Y., Valet, P., Gladine, C., Durand, T., et al. (2016). Simultaneous quantitative profiling of 20 isoprostanoids from omega-3 and omega-6 polyunsaturated fatty acids by LC-MS/MS in various biological samples. *Anal. Chim. Acta* **921**, 46–58.

Durand, T., Bultel-Poncé, V., Guy, A., Berger, S., Mueller, M. J. and Galano, J. M. (2009). New bioactive oxylipins formed by non-enzymatic free-radical-catalyzed pathways: The phytoprostanes. *Lipids* **44**, 875–888.

Epstein, H. E., Torda, G. and van Oppen, M. J. H. (2019). Relative stability of the Pocillopora acuta microbiome throughout a thermal stress event. *Coral Reefs* **38**, 373–386.

Fadhlaoui, M. and Lavoie, I. (2021). Effects of temperature and glyphosate on fatty acid composition, antioxidant capacity, and lipid peroxidation in the gastropod lymneae sp. *Water (Switzerland)* **13**,.

Fan, L., Liu, M., Simister, R., Webster, N. S. and Thomas, T. (2013). Marine microbial symbiosis heats up: the phylogenetic and functional response of a sponge holobiont to thermal stress. *ISME J.* **7**, 991–1002.

Feng, J., Zhang, L., Tang, X., Xia, X., Hu, W. and Zhou, P. (2021). Season and geography induced variation in sea cucumber (Stichopus japonicus) nutritional composition and gut microbiota. *J. Food Compos. Anal.* **101**, 103838.

Flannigan, K. L., McCoy, K. D. and Wallace, J. L. (2011). Eukaryotic and prokaryotic contributions to colonic hydrogen sulfide synthesis. *Am. J. Physiol. - Gastrointest. Liver Physiol.* **301**, 188–193.

Folch, J., Lees, M. and Sloane Stanley, G. H. (1957). A simple method for the isolation and purification of total lipides from animal tissues. *J. Biol. Chem.* **226**, 497–509.

Fontaine, S. S. and Kohl, K. D. (2022). The microbiome buffers tadpole hosts from heat stress : a hologenomic approach to understand host-microbe interactions under warming. *J. Exp. Biol.*

Fontaine, S. S., Mineo, P. M. and Kohl, K. D. (2022). Experimental manipulation of microbiota reduces host thermal tolerance and fitness under heat stress in a vertebrate ectotherm. *Nat. Ecol. Evol.* **6**, 405–417.

Foster, K. R., Schluter, J., Coyte, K. Z. and Rakoff-Nahoum, S. (2017). The evolution of the host microbiome as an ecosystem on a leash. *Nature* **548**, 43–51.

Fox, J. and Weisberg, S. (2019). *An R Companion to Applied Regression*.

Freire, C. A., Welker, A. F., Storey, J. M., Storey, K. B. and Hermes-lima, M. (2011). Oxidative Stress in Estuarine and Intertidal Environments (Temperate and Tropical). In *Oxidative Stress in Aquatic Ecosystems* (ed. Abele, D.), Pablo, J.), Vázquez-Medina), and Zenteno-Savín, T.), pp. 41–57. Blackwell Publishing Ltd.

Fu, Y., Wang, Y., Gao, H., Li, D., Jiang, R., Ge, L., Tong, C. and Xu, K. (2021). Associations among Dietary Omega-3 Polyunsaturated Fatty Acids, the Gut Microbiota,

and Intestinal Immunity. *Mediators Inflamm.* **2021**,.

Galano, J. M., Lee, Y. Y., Oger, C., Vigor, C., Vercauteren, J., Durand, T., Giera, M. and Lee, J. C. Y. (2017). Isoprostanes, neuroprostanes and phytoprostanes: An overview of 25 years of research in chemistry and biology. *Prog. Lipid Res.* **68**, 83–108.

Garren, M., Son, K., Tout, J., Seymour, J. R. and Stocker, R. (2016). Temperature-induced behavioral switches in a bacterial coral pathogen. *ISME J.* **10**, 1363–1372.

Garrity, S. D. (1984). Some Adaptations of Gastropods to Physical Stress on a Tropical Rocky Shore Author (s): Stephen D . Garrity Published by : Wiley Stable URL : http://www.jstor.org/stable/1941418 REFERENCES Linked references are available on JSTOR for this article : You. *Ecology* **65**, 559–574.

Giomi, F., Mandaglio, C., Ganmanee, M., Han, G. D., Dong, Y., Williams, G. A. and Sara, G. (2016). The importance of thermal history: Costs and benefits of heat exposure in a tropical, rocky shore oyster. *J. Exp. Biol.* **219**, 686–694.

Green, T. J. and Barnes, A. C. (2010). Bacterial diversity of the digestive gland of Sydney rock oysters, Saccostrea glomerata infected with the paramyxean parasite, Marteilia sydneyi. *J. Appl. Microbiol.* **109**, 613–622.

Hand, S. C. and Hardewig, I. (1996). Downregulation of cellular metabolism during environmental stress: Mechanisms and implications. *Annu. Rev. Physiol.* **58**, 539–563.

Harley, C. D. G. (2008). Tidal dynamics, topographic orientation, and temperature-mediated mass mortalities on rocky shores. *Mar. Ecol. Prog. Ser.* **371**, 37–46.

Hartman, L. M., van Oppen, M. J. H. and Blackall, L. L. (2020). The effect of thermal stress on the bacterial microbiome of exaiptasia diaphana. *Microorganisms* **8**, 1–18.

Helmuth, B. and Hofmann, G. E. (2001). Microhabitats, thermal heterogeneity, and patterns of physiological stress in the rocky intertidal zone. *Biol. Bull.* **201**, 374–384.

Herlemann, D. P. R., Labrenz, M., Jürgens, K., Bertilsson, S., Waniek, J. J. and Andersson, A. F. (2011). Transitions in bacterial communities along the 2000 km salinity gradient of the Baltic Sea. *ISME J.* **5**, 1571–1579.

Hermes-Lima, M. and Zenteno-Savín, T. (2002). Animal response to drastic changes in oxygen availability and physiological oxidative stress. *Comp. Biochem. Physiol. - C Toxicol. Pharmacol.* **133**, 537–556.

Hermes-Lima, M., Moreira, D. C., Rivera-Ingraham, G. A., Giraud-Billoud, M., Genaro-Mattos, T. C. and Campos, É. G. (2015). Preparation for oxidative stress under hypoxia and metabolic depression: Revisiting the proposal two decades later. *Free Radic. Biol. Med.* **89**, 1122–1143.

Herrera, M., Klein, S. G., Schmidt-Roach, S., Campana, S., Cziesielski, M. J., Chen, J. E., Duarte, C. M. and Aranda, M. (2020). Unfamiliar partnerships limit cnidarian holobiont acclimation to warming. *Glob. Chang. Biol.* **26**, 5539–5553.

Huang, Z., Yu, K., Fang, Y., Dai, H., Cai, H., Li, Z., Kan, B., Wei, Q. and Wang, D. (2020). Comparative Genomics and Transcriptomics Analyses Reveal a Unique Environmental Adaptability of Vibrio fujianensis. *Microorganisms* **8**, 555.

Hui, T. Y., Dong, Y., Han, G. D., Lau, S. L. Y., Cheng, M. C. F., Meepoka, C., Ganmanee, M. and Williams, G. A. (2020). Timing metabolic depression: Predicting thermal stress in extreme intertidal environments. *Am. Nat.* **196**, 501–511.

Huus, K. E. and Ley, R. E. (2021). Blowing Hot and Cold: Body Temperature and the Microbiome. *mSystems* **6**,.

Huyben, D., Roehe, B. K., Bekaert, M., Ruyter, B. and Glencross, B. (2020). Dietary Lipid:Protein Ratio and n-3 Long-Chain Polyunsaturated Fatty Acids Alters the Gut Microbiome of Atlantic Salmon Under Hypoxic and Normoxic Conditions. *Front. Microbiol.* **11**, 589898.

Imbusch, R. and Mueller, M. J. (2000). Analysis of oxidative stress and wound-inducible

897 dinor isoprostanes F1 (Phytoprostanes F1) in plants. *Plant Physiol.* **124**, 1293–1303.
898 **Jahn, U., Galano, J. M. and Durand, T.** (2008). Beyond prostaglandins - Chemistry and
899 biology of cyclic oxygenated metabolites formed by free-radical pathways from
900 polyunsaturated fatty acids. *Angew. Chemie - Int. Ed.* **47**, 5894–5955.
901 **Kandlikar, G. S., Gold, Z. J., Cowen, M. C., Meyer, R. S., Freise, A. C., Kraft, N. J. B.,**
902 **Moberg-Parker, J., Sprague, J., Kushner, D. J. and Curd, E. E.** (2018). Ranacapa:
903 An R package and shiny web app to explore environmental DNA data with exploratory
904 statistics and interactive visualizations. *F1000Research* **7**, 1–19.
905 **Klepac, C. N., Beal, J., Kenkel, C. D., Sproles, A., Polinski, J. M., Williams, M. A., Matz,**
906 **M. V. and Voss, J. D.** (2015). Seasonal stability of coral-Symbiodinium associations in
907 the subtropical coral habitat of St. Lucie Reef, Florida. *Mar. Ecol. Prog. Ser.* **532**, 137–
908 151.
909 **Klindworth, A., Pruesse, E., Schweer, T., Peplies, J., Quast, C., Horn, M. and Glöckner,**
910 **F. O.** (2013). Evaluation of general 16S ribosomal RNA gene PCR primers for classical
911 and next-generation sequencing-based diversity studies. *Nucleic Acids Res.* **41**, 1–11.
912 **Kodama, Y. and Watanabe, K.** (2004). Sulfuricurvum kujiense gen. nov., sp. nov., a
913 facultatively anaerobic, chemolithoautotrophic, sulfur-oxidizing bacterium isolated from
914 an underground crude-oil storage cavity. *Int. J. Syst. Evol. Microbiol.* **54**, 2297–2300.
915 **Kremer, N., Koch, E. J., El Filali, A., Zhou, L., Heath-Heckman, E. A. C., Ruby, E. G.**
916 **and McFall-Ngai, M. J.** (2018). Persistent Interactions with Bacterial Symbionts Direct
917 Mature-Host Cell Morphology and Gene Expression in the Squid-Vibrio Symbiosis.
918 *mSystems* **3**, 1–17.
919 **Lathlean, J. A., Ayre, D. J. and Minchinton, T. E.** (2014). Estimating latitudinal variability
920 in extreme heat stress on rocky intertidal shores. *J. Biogeogr.* **41**, 1478–1491.
921 **Lau, N. S., Ting, S. Y., Sam, K. K., Janaranjani, M., Wong, S. C., Wu, X., Waiho, K.,**
922 **Fazhan, H. and Shu-Chien, A. C.** (2022). Comparative Analyses of Scylla olivacea Gut
923 Microbiota Composition and Function Suggest the Capacity for Polyunsaturated Fatty
924 Acid Biosynthesis. *Microb. Ecol.* 1–14.
925 **Le Moullac, G., Cheize, M., Gastineau, O., Daniel, J. Y., Le Coz, J. R., Huvet, A., Moal,**
926 **J., Pouvreau, S., Van Wormhoudt, A. and Samain, J. F.** (2008). Ecophysiological and
927 metabolic adaptations to sulphide exposure of the oyster Crassostrea gigas. *J. Shellfish*
928 *Res.* **27**, 355–363.
929 **Lee, Y. Y. and Lee, J. C.-Y.** (2018). LC-MS/MS Analysis of Lipid Oxidation Products in
930 Blood and Tissue Samples. In *Clinical Metabolomics: Methods and Protocols* (ed.
931 Giera, M.), p. Springer Science+Business Media, LLC.
932 **Lee, Y. Y., Galano, J. M., Leung, H. H., Balas, L., Oger, C., Durand, T. and Lee, J. C. Y.**
933 (2020). Nonenzymatic oxygenated metabolite of docosahexaenoic acid, 4(RS)-4-F4t-
934 neuroprostane, acts as a bioactive lipid molecule in neuronal cells. *FEBS Lett.* **594**,
935 1797–1808.
936 **Lent, C. M.** (1969). Adaptations of the ribbed mussel, Modiolus demissus (Dillvvyn), to the
937 intertidal habitat. *Integr. Comp. Biol.* **9**, 283–292.
938 **Lenth, R. V.** (2023). emmeans: Estimated Marginal Means, aka Least-Squares Means.
939 **Letendre, J., Chouquet, B., Manduzio, H., Marin, M., Bultelle, F., Leboulenger, F. and**
940 **Durand, F.** (2009). Tidal height influences the levels of enzymatic antioxidant defences
941 in Mytilus edulis. *Mar. Environ. Res.* **67**, 69–74.
942 **Leung, K. S., Galano, J. M., Durand, T. and Lee, J. C. Y.** (2015). Current development in
943 non-enzymatic lipid peroxidation products, isoprostanoids and isofuranoids, in novel
944 biological samples. *Free Radic. Res.* **49**, 816–826.
945 **Li, Y. F., Yang, N., Liang, X., Yoshida, A., Osatomi, K., Power, D., Batista, F. M. and**
946 **Yang, J. L.** (2018). Elevated seawater temperatures decrease microbial diversity in the

gut of Mytilus coruscus. *Front. Physiol.* **9**, 839.
Li, J., Bates, K. A., Hoang, K. L., Hector, T. E., Knowles, S. C. L. and King, K. C. (2022). Experimental temperatures shape host microbiome diversity and composition. *Glob. Chang. Biol.* **00**, 1–16.
Lin, H. and Peddada, S. Das (2020). Analysis of compositions of microbiomes with bias correction. *Nat. Commun.* **11**, 1–11.
Loeffler, C., Berger, S., Guy, A., Durand, T., Bringmann, G., Dreyer, M., Von Rad, U., Durner, J. and Mueller, M. J. (2005). B1-phytoprostanes trigger plant defense and detoxification responses. *Plant Physiol.* **137**, 328–340.
Lokmer, A. and Mathias Wegner, K. (2015). Hemolymph microbiome of Pacific oysters in response to temperature, temperature stress and infection. *ISME J.* **9**, 670–682.
Longford, S. R., Campbell, A. H., Nielsen, S., Case, R. J., Kjelleberg, S. and Steinberg, P. D. (2019). Interactions within the microbiome alter microbial interactions with host chemical defences and affect disease in a marine holobiont. *Sci. Rep.* **9**, 1–13.
Lund, I. and Steenfeldt, S. J. (2011). The effects of dietary long-chain essential fatty acids on growth and stress tolerance in pikeperch larvae (Sander lucioperca L.). *Aquac. Nutr.* **17**, 191–199.
Ma, K., Chen, S., Wu, Y., Ma, Y., Qiao, H., Fan, J. and Wu, H. (2022). Dietary supplementation with microalgae enhances the zebrafish growth performance by modulating immune status and gut microbiota. *Appl. Microbiol. Biotechnol.* **106**, 773–788.
Maher, R. L., Schmeltzer, E. R., Meiling, S., McMinds, R., Ezzat, L., Shantz, A. A., Adam, T. C., Schmitt, R. J., Holbrook, S. J., Burkepile, D. E., et al. (2020). Coral Microbiomes Demonstrate Flexibility and Resilience Through a Reduction in Community Diversity Following a Thermal Stress Event. *Front. Ecol. Evol.* **8**, 555698.
Mallott, E. K., Skovmand, L. H., Garber, P. A. and Amato, K. R. (2022). *The fecal metabolome of black howler monkeys (Alouatta pigra) varies in response to seasonal dietary changes* .
Marangon, E., Laffy, P. W., Bourne, D. G. and Webster, N. S. (2021). Microbiome-mediated mechanisms contributing to the environmental tolerance of reef invertebrate species. *Mar. Biol.* **168**, 1–18.
Marshall, D. J. and McQuaid, C. D. (2011). Warming reduces metabolic rate in marine snails: Adaptation to fluctuating high temperatures challenges the metabolic theory of ecology. *Proc. R. Soc. B Biol. Sci.* **278**, 281–288.
Marshall, D. J. and McQuaid, C. D. (2020). Metabolic Regulation, Oxygen Limitation and Heat Tolerance in a Subtidal Marine Gastropod Reveal the Complexity of Predicting Climate Change Vulnerability. *Front. Physiol.* **11**, 1106.
Marshall, D. J., Dong, Y., McQuaid, C. D. and Williams, G. A. (2011). Thermal adaptation in the intertidal snail Echinolittorina malaccana contradicts current theory by revealing the crucial roles of resting metabolism. *J. Exp. Biol.* **214**, 3649–3657.
McDevitt-Irwin, J. M., Garren, M., McMinds, R., Vega Thurber, R. and Baum, J. K. (2019). Variable interaction outcomes of local disturbance and El Niño-induced heat stress on coral microbiome alpha and beta diversity. *Coral Reefs* **38**, 331–345.
McKnight, D. T., Huerlimann, R., Bower, D. S., Schwarzkopf, L., Alford, R. A. and Zenger, K. R. (2019). Methods for normalizing microbiome data: An ecological perspective. *Methods Ecol. Evol.* **10**, 389–400.
Mcmahon, B. R. (1988). Physiological responses to oxygen depletion in intertidal animals. *Integr. Comp. Biol.* **28**, 39–53.
McMurdie, P. J. and Holmes, S. (2013). Phyloseq: An R Package for Reproducible Interactive Analysis and Graphics of Microbiome Census Data. *PLoS One* **8**,.

997 **Miller, E., Morel, A., Saso, L. and Saluk, J.** (2014). Isoprostanes and neuroprostanes as
998 biomarkers of oxidative stress in neurodegenerative diseases. *Oxid. Med. Cell. Longev.*
999 **2014**,.
1000 **Moghadam, N. N., Thorshauge, P. M., Kristensen, T. N., de Jonge, N., Bahrndorff, S.,**
1001 **Kjeldal, H. and Nielsen, J. L.** (2018). Strong responses of Drosophila melanogaster
1002 microbiota to developmental temperature. *Fly (Austin).* **12**, 1–12.
1003 **Muñoz, K., Flores-Herrera, P., Gonçalves, A. T., Rojas, C., Yáñez, C., Mercado, L.,**
1004 **Brokordt, K. and Schmitt, P.** (2019). The immune response of the scallop Argopecten
1005 purpuratus is associated with changes in the host microbiota structure and diversity. *Fish*
1006 *Shellfish Immunol.* **91**, 241–250.
1007 **Nakagawa, S., Saito, H., Tame, A., Hirai, M., Yamaguchi, H., Sunata, T., Aida, M.,**
1008 **Muto, H., Sawayama, S. and Takaki, Y.** (2017). Microbiota in the coelomic fluid of
1009 two common coastal starfish species and characterization of an abundant Helicobacter-
1010 related taxon. *Sci. Rep.* **7**, 1–10.
1011 **Narrowe, A. B., Albuthi-Lantz, M., Smith, E. P., Bower, K. J., Roane, T. M., Vajda, A.**
1012 **M. and Miller, C. S.** (2015). Perturbation and restoration of the fathead minnow gut
1013 microbiome after low-level triclosan exposure. *Microbiome* **3**, 1–18.
1014 **Nearing, J. T., Douglas, G. M., Hayes, M., Macdonald, J., Desai, D., Allward, N., Jones,**
1015 **C. M. A., Wright, R., Dhanani, A., Comeau, A. M., et al.** (2022). Microbiome
1016 differential abundance methods produce disturbingly different results across 38 datasets.
1017 *Nat. Commun.* **13**, 342.
1018 **Neu, A. T., Hughes, I. V., Allen, E. E. and Roy, K.** (2021). Decade-scale stability and
1019 change in a marine bivalve microbiome. *Mol. Ecol.* **30**, 1237–1250.
1020 **Ng, T. P. T., Lau, S. L. Y., Seuront, L., Davies, M. S., Stafford, R., Marshall, D. J. and**
1021 **Williams, G. A.** (2017). Linking behaviour and climate change in intertidal ectotherms:
1022 insights from littorinid snails. *J. Exp. Mar. Bio. Ecol.* **492**, 121–131.
1023 **Ng, T. P. T., Lau, S. L. Y., Davies, M. S., Stafford, R., Seuront, L., Hutchinson, N., Hui,**
1024 **T. T. Y. and Williams, G. A.** (2021). Behavioral repertoire of high-shore littorinid
1025 snails reveals novel adaptations to an extreme environment. *Ecol. Evol.* **11**, 7114–7124.
1026 **Nguyen, Q. P., Karagas, M. R., Madan, J. C., Dade, E., Palys, T. J., Morrison, H. G.,**
1027 **Pathmasiri, W. W., McRitche, S., Sumner, S. J., Frost, H. R., et al.** (2021).
1028 Associations between the gut microbiome and metabolome in early life. *BMC Microbiol.*
1029 **21**, 1–19.
1030 **Nicastro, K. R., Zardi, G. I., McQuaid, C. D., Stephens, L., Radloff, S. and Blatch, G. L.**
1031 (2010). The role of gaping behaviour in habitat partitioning between coexisting intertidal
1032 mussels. *BMC Ecol.* **10**,.
1033 **Oksanen, J., Simpson, G. L., Blanchet, F. G., Kindt, R., Legendre, P., Minchin, P. R.,**
1034 **O'Hara, R. B., Solymos, P., Stevens, M. H. H., Szoecs, E., et al.** (2022). vegan:
1035 community ecology package. *R Packag. version 2.6-2*.
1036 **Paix, B., Othmani, A., Debroas, D., Culioli, G. and Briand, J. F.** (2019). Temporal
1037 covariation of epibacterial community and surface metabolome in the Mediterranean
1038 seaweed holobiont Taonia atomaria. *Environ. Microbiol.* **21**, 3346–3363.
1039 **Pal, V. K., Bandyopadhyay, P. and Singh, A.** (2018). Hydrogen sulfide in physiology and
1040 pathogenesis of bacteria and viruses. *IUBMB Life* **70**, 393–410.
1041 **Parris, D. J., Morgan, M. M. and Stewart, F. J.** (2019). Feeding rapidly alters microbiome
1042 composition and gene transcription in the clownfish gut. *Appl. Environ. Microbiol.* **85**,
1043 1–15.
1044 **Pernet, F., Tremblay, R., Redjah, I., Sévigny, J. M. and Gionet, C.** (2008). Physiological
1045 and biochemical traits correlate with differences in growth rate and temperature
1046 adaptation among groups of the eastern oyster Crassostrea virginica. *J. Exp. Biol.* **211**,

969–977.
Pierce, M. L. and Evan, J. (2019). Gut microbiomes of the eastern oyster (Crassostrea virginica) and the blue mussel (Mytilus edulis): temporal variation and the influence of marine aggregate-associated microbial communities. *mSphere* **4**, e00730-19.
Pimentel, Z. T., Dufault-Thompson, K., Russo, K. T., Scro, A. K., Smolowitz, R. M., Gomez-Chiarri, M. and Zhang, Y. (2021). Microbiome Analysis Reveals Diversity and Function of Mollicutes Associated with the Eastern Oyster, Crassostrea virginica. *mSphere* **6**, e00227-21.
Pita, L., Rix, L., Slaby, B. M., Franke, A. and Hentschel, U. (2018). The sponge holobiont in a changing ocean: from microbes to ecosystems. *Microbiome* **6**, 46.
Quast, C., Pruesse, E., Yilmaz, P., Gerken, J., Schweer, T., Yarza, P., Peplies, J. and Glöckner, F. O. (2013). The SILVA ribosomal RNA gene database project: Improved data processing and web-based tools. *Nucleic Acids Res.* **41**, D590–D596.
Rädecker, N., Pogoreutz, C., Gegner, H. M., Cárdenas, A., Perna, G., Geißler, L., Roth, F., Bougoure, J., Guagliardo, P., Struck, U., et al. (2022). Heat stress reduces the contribution of diazotrophs to coral holobiont nitrogen cycling. *ISME J.* **16**, 1110–1118.
Raffaelli, D. and Hawkins, S. (1999). *Intertidal ecology*. 2nd ed. Kluwer Academic Publishers.
Rivera-Ingraham, G. A., Rocchetta, I., Meyer, S. and Abele, D. (2013). Oxygen radical formation in anoxic transgression and anoxia-reoxygenation: Foe or phantom? Experiments with a hypoxia tolerant bivalve. *Mar. Environ. Res.* **92**, 110–119.
Rocca, J. D., Simonin, M., Blaszczak, J. R., Ernakovich, J. G., Gibbons, S. M., Midani, F. S. and Washburne, A. D. (2019). The Microbiome Stress Project: Toward a global meta-analysis of environmental stressors and their effects on microbial communities. *Front. Microbiol.* **9**, 3272.
Roy, J., Galano, J. M., Durand, T., Le Guennec, J. Y. and Lee, J. C. Y. (2017). Physiological role of reactive oxygen species as promoters of natural defenses. *FASEB J.* **31**, 3729–3745.
Samakraman, S., Williams, G. A. and Ganmanee, M. (2010). Spatial and Temporal Variability of Intertidal Rocky Shore Molluscs in Sichang Island, East Coast of Thailand. *Publ. Seto Mar. Biol. Lab.* **10**, 35–46.
Santoro, E. P., Borges, R. M., Espinoza, J. L., Freire, M., Messias, C. S. M. A., Villela, H. D. M., Pereira, L. M., Vilela, C. L. S., Rosado, J. G., Cardoso, P. M., et al. (2021). Coral microbiome manipulation elicits metabolic and genetic restructuring to mitigate heat stress and evade mortality. *Sci. Adv.* **7**, 19–21.
Sargent, J. R. (1976). The Structure, Metabolism and Function of Lipids in Marine organisms. In *Biochemical and biophysical perspectives in marine biology* (ed. Malins, D. C.) and Sargent, J. R.), pp. 149–212. New York: Academic Press.
Shankar, V., Homer, D., Rigsbee, L., Khamis, H. J., Michail, S., Raymer, M., Reo, N. V. and Paliy, O. (2015). The networks of human gut microbe-metabolite associations are different between health and irritable bowel syndrome. *ISME J.* **9**, 1899–1903.
Sharp, C. and Foster, K. R. (2022). Host control and the evolution of cooperation in host microbiomes. *Nat. Commun.* **13**, 1–15.
Sharp, K. H., Pratte, Z. A., Kerwin, A. H., Rotjan, R. D. and Stewart, F. J. (2017). Season, but not symbiont state, drives microbiome structure in the temperate coral Astrangia poculata. *Microbiome* **5**, 120.
Shaver, E. C., Shantz, A. A., McMinds, R., Burkepile, D. E., Thurber, R. L. V. and Silliman, B. R. (2017). Effects of predation and nutrient enrichment on the success and microbiome of a foundational coral. *Ecology* **98**, 830–839.
Shiu, J. H., Keshavmurthy, S., Chiang, P. W., Chen, H. J., Lou, S. P., Tseng, C. H.,

Justin Hsieh, H., Allen Chen, C. and Tang, S. L. (2017). Dynamics of coral-associated bacterial communities acclimated to temperature stress based on recent thermal history. *Sci. Rep.* **7**, 1–13.

Soen, Y. (2014). Environmental disruption of host-microbe co-adaptation as a potential driving force in evolution. *Front. Genet.* **5**, 168.

Sokolova, I. M. and Pörtner, H. O. (2001). Physiological adaptations to high intertidal life involve improved water conservation abilities and metabolic rate depression in littorina saxatilis. *Mar. Ecol. Prog. Ser.* **224**, 171–186.

Somero, G. N. (2002). Thermal physiology and vertical zonation of intertidal animals: Optima, limits, and costs of living. *Integr. Comp. Biol.* **42**, 780–789.

Sorek, M., Díaz-Almeyda, E. M., Medina, M. and Levy, O. (2014). Circadian clocks in symbiotic corals: The duet between Symbiodinium algae and their coral host. *Mar. Genomics* **14**, 47–57.

Stillman, J. H. (2002). Causes and consequences of thermal tolerance limits in rocky intertidal porcelain crabs, genus Petrolisthes. *Integr. Comp. Biol.* **42**, 790–796.

Storey, K. B. and Storey, J. M. (2004). Oxygen Limitation and Metabolic Rate Depression. In *Functional Metabolism: Regulation and Adaptation*, p. John Wiley & Sons, Inc.

Sussarellu, R., Fabioux, C., Camacho Sanchez, M., Le Goïc, N., Lambert, C., Soudant, P. and Moraga, D. (2012). Molecular and cellular response to short-term oxygen variations in the Pacific oyster Crassostrea gigas. *J. Exp. Mar. Bio. Ecol.* **412**, 87–95.

Thoma, I., Loeffler, C., Sinha, A. K., Gupta, M., Krischke, M., Steffan, B., Roitsch, T. and Mueller, M. J. (2003). Cyclopentenone isoprostanes induced by reactive oxygen species trigger defense gene activation and phytoalexin accumulation in plants. *Plant J.* **34**, 363–375.

Tignat-Perrier, R., van de Water, J. A. J. M., Guillemain, D., Aurelle, D., Allemand, D. and Ferrier-Pagès, C. (2022). The Effect of Thermal Stress on the Physiology and Bacterial Communities of Two Key Mediterranean Gorgonians. *Appl. Environ. Microbiol.* **88**,.

Vandamme, P. and De Ley, J. (1991). Proposal for a new family, Campylobacteraceae. *Int. J. Syst. Bacteriol.* **41**, 451–455.

Voolstra, C. R. and Ziegler, M. (2020). Adapting with Microbial Help: Microbiome Flexibility Facilitates Rapid Responses to Environmental Change. *BioEssays* **42**, 1–9.

Walke, J. B., Becker, M. H., Krinos, A., Chang, E. A. B., Santiago, C., Umile, T. P., Minbiole, K. P. C. and Belden, L. K. (2021). Seasonal changes and the unexpected impact of environmental disturbance on skin bacteria of individual amphibians in a natural habitat. *FEMS Microbiol. Ecol.* **97**, 1–14.

Wang, J., Ren, R. M. and Yao, C. L. (2018). Oxidative stress responses of Mytilus galloprovincialis to acute cold and heat during air exposure. *J. Molluscan Stud.* **84**, 285–292.

Wang, J., Ma, L. X. and Dong, Y. W. (2022). Coping with harsh heat environments: molecular adaptation of metabolic depression in the intertidal snail Echinolittorina radiata. *Cell Stress Chaperones*.

Webster, N. S., Cobb, R. E. and Negri, A. P. (2008). Temperature thresholds for bacterial symbiosis with a sponge. *ISME J.* **2**, 830–842.

Weiss, S., Xu, Z. Z., Peddada, S., Amir, A., Bittinger, K., Gonzalez, A., Lozupone, C., Zaneveld, J. R., Vázquez-Baeza, Y., Birmingham, A., et al. (2017). Normalization and microbial differential abundance strategies depend upon data characteristics. *Microbiome* **5**, 1–18.

Welker, A. F., Moreira, D. C., Campos, É. G. and Hermes-Lima, M. (2013). Role of redox metabolism for adaptation of aquatic animals to drastic changes in oxygen

availability. *Comp. Biochem. Physiol. - A Mol. Integr. Physiol.* **165**, 384–404.
Wickham, H. (2008). *ggplot2: Elegant Graphics for Data Analysis*. New York, USA: Springer Science+Business Media, LCC.
Williams, G. A. and Morritt, D. (1995). Habitat partitioning and thermal tolerance in a tropical limpet, Cellana grata. *Mar. Ecol. Prog. Ser.* **124**, 89–103.
Yin, X., Chen, P., Chen, H., Jin, W. and Yan, X. (2017). Physiological performance of the intertidal Manila clam (Ruditapes philippinarum) to long-term daily rhythms of air exposure. *Sci. Rep.* **7**, 41648.
Yonny, M. E., Rodríguez Torresi, A., Cuyamendous, C., Réversat, G., Oger, C., Galano, J. M., Durand, T., Vigor, C. and Nazareno, M. A. (2016). Thermal Stress in Melon Plants: Phytoprostanes and Phytofurans as Oxidative Stress Biomarkers and the Effect of Antioxidant Supplementation. *J. Agric. Food Chem.* **64**, 8296–8304.
Zaneveld, J. R., McMinds, R. and Thurber, R. V. (2017). Stress and stability: Applying the Anna Karenina principle to animal microbiomes. *Nat. Microbiol.* **2**,.
Zhou, K., Aertsen, A. and Michiels, C. W. (2014). The role of variable DNA tandem repeats in bacterial adaptation. *FEMS Microbiol. Rev.* **38**, 119–141.
Zhukova, N. V. (2019). Fatty acids of marine mollusks: Impact of diet, bacterial symbiosis and biosynthetic potential. *Biomolecules* **9**, 1–25.
Ziegler, M., Seneca, F. O., Yum, L. K., Palumbi, S. R. and Voolstra, C. R. (2017). Bacterial community dynamics are linked to patterns of coral heat tolerance. *Nat. Commun.* **8**, 1–8.

Supplementary information

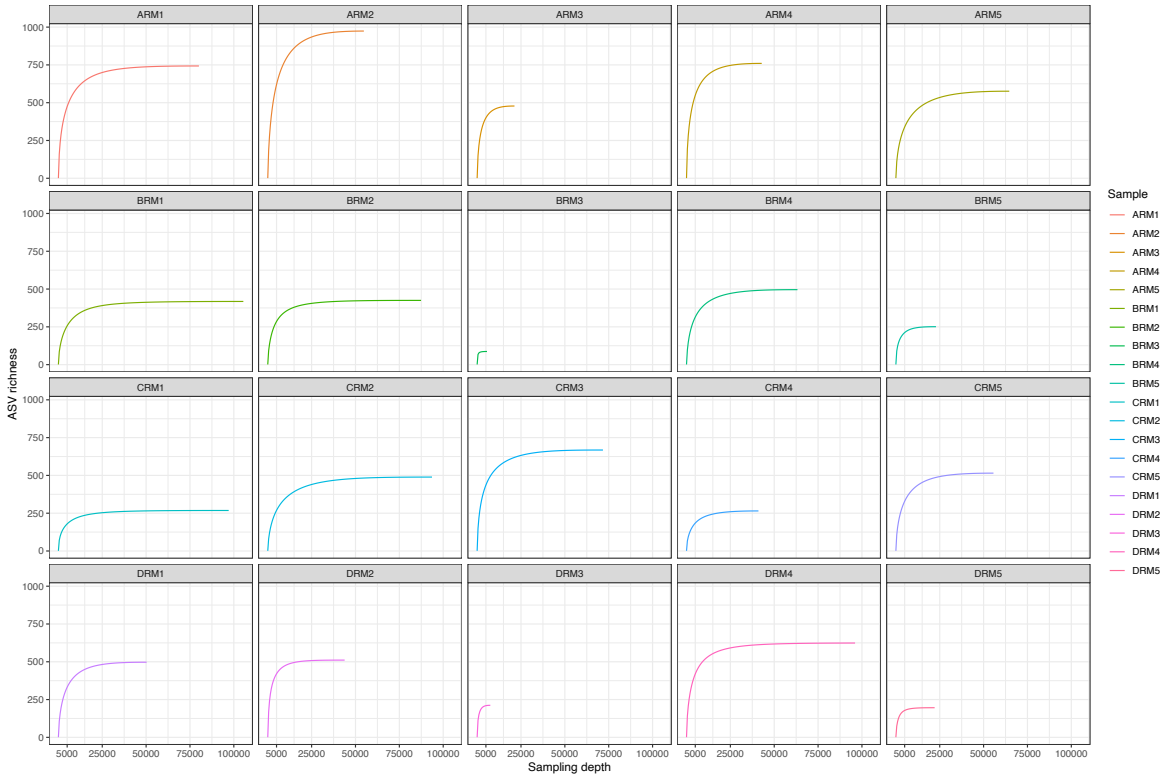

Fig. S1. Rarefaction curves illustrating the ASVs captured against the sampling depth which was generated for each sample using their corresponding quality-filtered V3-V4 16SrRNA sequences.

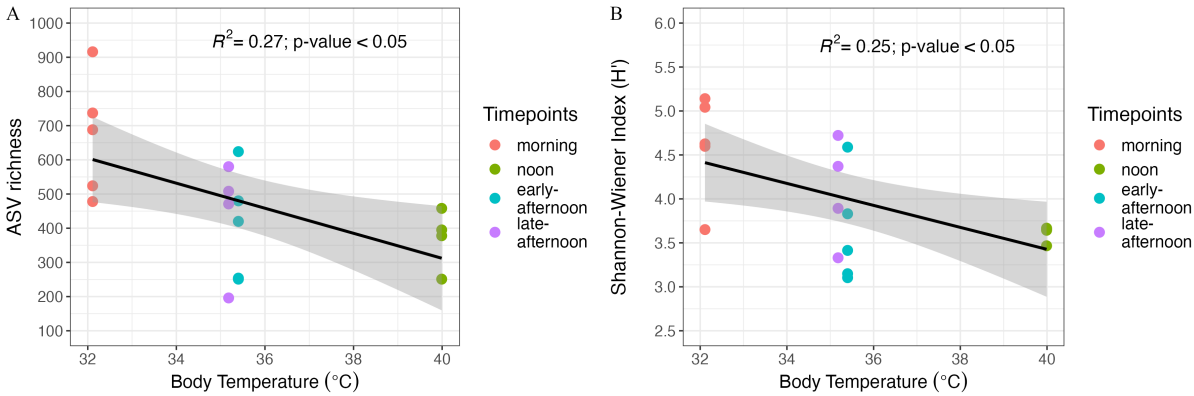

Fig. S2. Variation in the alpha diversity indices of the *I. nucleus*-associated microbiome can be explained by the host body temperature. Linear regression graph showing the relationship between average body temperature (from 10 random independent replicates collected at each timepoint) and (A) ASV richness (B) Shannon-Wiener index (H'). The datapoints shown in each panel were the samples' replicates (n= 4-5) from their corresponding timepoint. The shaded grey area indicates a 95% confidence interval for the predicted regression line. Statistical result (least square regression analysis) is shown in the upper right within each panel.

Table S1. Metadata describing the *Isognomon nucleus* samples' collected information

Date	Time	Timepoints label	Replicates	Sample name	Body (mm)
22.05.2019	0915	morning	1	ARM1	12.9
22.05.2019	0915	morning	2	ARM2	13.5
22.05.2019	0915	morning	3	ARM3	15.2
22.05.2019	0915	morning	4	ARM4	12.5
22.05.2019	0915	morning	5	ARM5	13.7
22.05.2019	1230	noon	1	BRM1	11.7
22.05.2019	1230	noon	2	BRM2	11.3
22.05.2019	1230	noon	3	BRM3	12.9
22.05.2019	1230	noon	4	BRM4	11.9
22.05.2019	1230	noon	5	BRM5	12.4
22.05.2019	1612	early-afternoon	1	CRM1	11.7
22.05.2019	1612	early-afternoon	2	CRM2	12.9
22.05.2019	1612	early-afternoon	3	CRM3	13.0
22.05.2019	1612	early-afternoon	4	CRM4	12.0
22.05.2019	1612	early-afternoon	5	CRM5	11.7
22.05.2019	1740	late-afternoon	1	DRM1	11.8
22.05.2019	1740	late-afternoon	2	DRM2	10.9
22.05.2019	1740	late-afternoon	3	DRM3	14.9
22.05.2019	1740	late-afternoon	4	DRM4	11.1
22.05.2019	1740	late-afternoon	5	DRM5	11.9